

Observation of different scenarios in different temperatures in small and large collision systems

Muhammad Waqas^{1*}, Lu-Meng Liu^{2†}, Guang-Xiong Peng^{1,3,4‡}, Muhammad Ajaz^{5§}

¹ *School of Nuclear Science and Technology, University of Chinese Academy of Sciences, Beijing 100049, People's Republic of China*

² *School of Physical Sciences, University of Chinese Academy of Sciences, Beijing 100049, China*

³ *Theoretical Physics Center for Science Facilities, Institute of High Energy Physics, Beijing 100049, China*

⁴ *Synergetic Innovation Center for Quantum Effects & Applications, Hunan Normal University, Changsha 410081, China*

⁵ *Department of Physics, Abdul Wali Khan University Mardan, 23200 Mardan, Pakistan*

Abstract: We used the modified Hagedron function and analyzed the experimental data measured by the BRAHMS, STAR, PHENIX and ALICE Collaborations in Copper-Copper, Gold-Gold, deuteron-Gold, Lead-Lead, proton-Lead and proton-proton collisions, and extracted the related parameters (kinetic freeze-out temperature, transverse flow velocity, kinetic freeze-out volume, mean transverse momentum and initial temperature) from the transverse momentum spectra of the particles (non-strange and strange particles). We observed that all the above parameters decrease from central to peripheral collisions, except transverse flow velocity which remains unchanged from central to peripheral collisions. The kinetic freeze-out temperature depends on the cross-section interaction of the particle such that larger cross-section of the particle corresponds to smaller T_0 , and reveals the two kinetic freeze-out scenario, while the initial temperature depends on the mass of the particle and it increase with the particle mass. The transverse flow velocity and mean transverse momentum depends on the mass of the particle and the former decrease while the later increase with the particle mass. In addition, the kinetic freeze-out volume also decrease with particle mass which reveals the volume differential freeze-out scenario and indicates different freeze-out surfaces for different particles. We also extracted the entropy index-parameter n and the parameter N_0 , and the former remains almost unchanged while the later decrease from central to peripheral collisions. Furthermore, the kinetic freeze-out temperature, transverse flow velocity, kinetic freeze-out volume, initial temperature, mean transverse momentum and the parameter N_0 at LHC are larger than that of RHIC, and they show their dependence on the collision cross-section as well as on collision energy at RHIC and LHC.

Keywords: bulk properties of nuclear matter; transverse momentum spectra; strange and non-strange particles; kinetic freeze-out temperature; initial temperature; kinetic freeze-out volume.

PACS numbers: 12.40.Ee, 13.85.Hd, 24.10.Pa

I. INTRODUCTION

A suitable tool for the production of the hot and dense matter namely Quark-Gluon Plasma (QGP) in the lab-

oratory [1, 2] is the high energy collisions. This state of matter is formed in the initial stages of collision, and it survives for a short period of time (7-10 fm/c) and then rapidly transforms into a hadron gas system. Because of the multi-partonic interactions throughout the evolution of the collision, the information about the initial condition of the system gets lost. In order to obtain the final state behavior of such a colliding system, we need the measurement of number and identity of the produced particles along with their energy and momentum spectra.

*waqas_phy313@yahoo.com, waqas_phy313@ucas.ac.cn

†liulumeng18@mails.ucas.ac.cn

‡Correspondence: gxpeng@ucas.edu.ac.cn

§Correspondence: ajaz@awakum.edu.pk, muhammad.ajaz@cern.ch

The final state information are very useful to understand the production mechanism of particles and the nature of produced matter in these high energy collisions.

The chemical and kinetic freeze-out are the two symbolic freeze-out conditions where the space-time evolution of the fireball produced in the collision cease. The colliding medium first reaches chemical equilibrium, where the inelastic scattering stops due to expansion of the system which results in the stabilization of the particle chemistry in the fireball. This stage is called chemical freeze-out stage and the temperature at this stage is known as chemical freeze-out temperature (T_{ch}) [4]. The relative fractions of the particles are fixed but they still interact with each other, and then stops until the final state interactions between them are no longer effective. This stage is called thermal/kinetic freeze-out stage and the temperature at this stage is known as kinetic freeze-out temperature [5–8]. In Standard model of heavy ion collisions, the kinetic freeze-out occurs after the chemical freeze-out due to large mean free path of the later which is also claimed in ref. [9]. Generally, the transverse momentum (p_T) spectra as well as the yields of the produced hadrons constitute some basic measurements for the extraction of parameters of chemical and kinetic freeze-out.

A multiple chemical freeze-out scenario with the early fixing of chemical composition of strange hadron compared to non-strange light hadrons is advocated in ref. [10]. The early chemical freeze-out of strange hadrons is due to their small inelastic cross-section. A natural question arise in mind whether a similar hierarchy structure also occurs at kinetic decoupling, or the mass dependent hierarchy occurs in case of kinetic freeze-out because the variation in medium induced momentum for heavy hadrons would be smaller than the lighter hadrons and therefore, with the decrease of temperature of the fireball, the earlier kinetic decoupling of heavy hadrons is expected.

In the present article, we will analyze the bulk properties in terms of kinetic freeze-out temperature (T_0), transverse flow velocity (β_T) and kinetic freeze-out volume (V). All these mentioned parameters are discussed in detail in various literatures [11–14]. In the present work, we choose different collision systems such as small and large systems in order to check the dependence of the above parameters on the size of interacting system and different particles are chosen in order to check the differences in different particle emissions.

Before going to the next section, we would like to point out that we also analyse the initial temperature

which occurs in the initial stage of collisions and which is also important to study because the phenomenon in the initial stages of collisions and the freeze-out stages is different.

The remainder of the paper consists of formalism and method, results discussions and conclusions.

II. FORMALISM AND METHOD

The structure of transverse momentum spectra (p_T) of the charged particles is very complex, and therefore is distributed into various regions. Especially, when the p_T range approaches to 100 GeV/c at LHC collisions [15]. There are different p_T regions according to the model analysis [16]. The first p_T region include $p_T < 4$ -6 GeV/c and second region include 4 -6 GeV/c $< p_T < 17$ -20 GeV/c, while the third region includes $p_T > 17$ -20 GeV/c. It is believed that different p_T regions (soft, hard and very hard p_T region) signify different interacting mechanisms. There are different explanations due to different models and methods even for the same p_T region. In the present work, the maximum p_T range is 7-8 GeV/c, therefore we will be limited to the soft and hard process and will skip the very hard process. There is a very soft region also which will be also skipped and it corresponds to $p_T < 0.5$ GeV/c which involves the resonance production that is not described by the model, but one can read ref. [17, 18] for more details of very soft and very hard processes. Generally, the soft excitation process is distributed in a narrow p_T range of less than 2-3 GeV/c or a little more, and mostly light flavor particles are produced in this region. The soft process have many choices of formalisms such as Blast wave model with Boltzmann Gibb's statistics [19–22], Blast wave model with Tsallis statistics [23–26], Tsallis pareto-type function [27], Erlang distribution [28–30], Scwinger mechanism [31–34], Hagedorn distribution function [35], Standard distribution [36] etc. The p_T region above 3 GeV/c is contributed for the hard process and is described by Quantum chromodynamics (QCD) calculus [37–39] or inverse power law which is also known as Hagedron function

$$f_0(p_T) = \frac{1}{N} \frac{dN}{dp_T} = A p_T \left(1 + \frac{p_T}{p_0} \right)^{-n}, \quad (1)$$

where A , is the normalization constant, and p_0 and n are free parameters. This function is revised in different forms in [40–45] and each has different significance.

In the present work, we use the Hagedorn function with embeded transverse flow velocity [46], which can be

expressed as

$$f_0(p_T) = \frac{1}{N} \frac{dN}{dp_T} = 2\pi C p_T \left[1 + \langle \gamma_t \rangle \frac{(m_T - p_T < \beta_T >)}{nT_0} \right]^{-n} \quad (2)$$

where C stands for the normalization constant that leads the integral in Eq. (2) to be normalized to 1, m_T is the transverse mass and is equal to $\sqrt{p_T^2 + m_0^2}$, m_0 is the rest mass of the particle, In Eq. 2, $C = gV/(2\pi)^2$. So Eq. 2 becomes as

$$f_0(p_T) = \frac{1}{N} \frac{dN}{dp_T} = \frac{gV}{2\pi} p_T \left[1 + \langle \gamma_t \rangle \frac{(m_T - p_T < \beta_T >)}{nT_0} \right]^{-n} \quad (3)$$

where g is the degeneracy factor which differs for every particle, depends on their spin based on $g_n = 2S_n + 1$.

III. RESULTS AND DISCUSSION

A. Comparison with data

Figure 1 shows the p_T spectra ($1/N_{ev}[(1/2\pi m_T) d^2N/dy dm_T]$ or $(1/2\pi p_T) d^2N/dy dp_T$) of π^+ , π^- , K^+ , K^- , p , \bar{p} , Λ and Ξ in Copper-Copper (Cu-Cu) collisions at 200 GeV in different centrality bins. The centrality intervals for π^+ , π^- , K^+ , K^- , p and \bar{p} are 0 – 10%, 10 – 30%, 30 – 50% and 50 – 70%. The centrality intervals for π^+ and π^- 10 – 30%, 30 – 50% and 50 – 70% are scaled by 1/2, 1/4 and 1/6 respectively, while for K^+ and K^- 30 – 50% and 50 – 70% are scaled by 0.3. For p and \bar{p} the centrality bins 10 – 30%, 30 – 50% and 50 – 70% are scaled by 0.4, 0.3 and 0.2 respectively. The centrality intervals for Λ and Ξ are 0 – 10%, 10 – 20%, 20 – 30%, 30 – 40% and 40 – 60%. π^+ , π^- , K^+ , K^- , p and \bar{p} are measured at $y = 0$, while for Λ and Ξ $|y| < 0.5$. The symbols are used to represent the experimental data of RHIC measured by the BRAHMS Collaboration, while the curves are our fit results by using the Modified Hagedorn function with embedded transverse flow i.e Eq. (3). The data/fit ratio is given in the figure followed by each panel. It can be seen that Eq. (3) fits the data approximately well. In some cases the fit in the p_T range up to 0.5 GeV/c is not good due to the resonance effect. The data for π^+ , π^- , K^+ , K^- , p , \bar{p} are taken from ref. [47], while for Λ and Ξ is from ref. [48].

Fig. 2 is similar to fig.1, but it shows the p_T spectra of π^+ , K^+ , p , Λ and Ξ^- in Au-Au collisions at 62.4 GeV.

The centrality is distributed in 0 – 5%, 0 – 10%, 10 – 20%, 20 – 30%, 30 – 40%, 40 – 50%, 50 – 60%, 60 – 70% and 70 – 80% intervals for π^+ , K^+ and p and the centrality bins 0 – 10%, 10 – 20%, 20 – 30%, 30 – 40%, 40 – 50%, 50 – 60%, 60 – 70% and 70 – 80% are scaled by 1/4, 1/15, 1/50, 1/80, 1/500, 1/1300, 1/2700 and 1/5400 respectively. Λ is distributed into 0 – 5%, 0 – 10%, 10 – 20%, 20 – 30%, 30 – 40%, 40 – 60% and 60 – 80% centrality intervals, while the centrality distribution for Ξ^- is 0 – 5%, 0 – 10%, 10 – 20%, 20 – 30%, 30 – 40% and 40 – 60%. One can see that the measurement of the STAR Collaboration is well fitted by the modified Hagedorn function. The data/fit ratio is followed in each panel in the figure. The data for π^+ , K^+ and p are taken from ref. [49], while for Λ and Ξ is taken from ref. [50].

The p_T spectra of the given particles are demonstrated in fig.3 and 4 in Deuteron-Gold (d-Au) collisions at 200 GeV and in Lead-Lead (Pb-Pb) collisions at 2.76 TeV respectively. In d-Au collisions π^+ , π^- , K^+ , K^- , p and \bar{p} , and in Pb-Pb collisions π^+ , K^+ , p , Λ and Ξ are analyzed. The centrality in d-Au is distributed in various centrality classes such that 0 – 20%, 20 – 40%, 40 – 60% and 60 – 88%. However the centrality for π^+ , π^- , K^+ , K^- , p and \bar{p} in Pb-Pb collisions is distributed in 0 – 5%, 0 – 10%, 10 – 20%, 20 – 30%, 30 – 40%, 40 – 50%, 50 – 60%, 60 – 70%, 70 – 80% and 80 – 90%, and except 0 – 5%, the other centrality bins are scaled by 1/2, 1/5, 1/10, 1/19, 1/36, 1/50, 1/70, 1/78 and 1/88 respectively. The centrality bins for Λ and Ξ are 0 – 10%, 10 – 20%, 20 – 40%, 40 – 60% and 60 – 80% and except 0 – 10%, the remaining centrality class are scaled by 1/2, 1/4, 1/6 and 1/8 respectively. The well fitting results of the model to the experimental data of ALICE collaboration can be seen, and the data/fit ratio are followed in each panel. The data in fig. 3 are taken from ref. [51], while in fig.4 for π^+ , π^- , K^+ , K^- , p and \bar{p} is taken from ref. [52], and Λ and Ξ^- are taken from ref. [53].

Fig.5 shows the p_T of the given particles in proton-Lead (p-Pb) and proton-proton (pp) collisions. Panel (a)-(d) shows the p_T spectra of the particles in p-Pb collisions in different centrality intervals at 5.02 TeV, and panel (e) represent the p_T spectra of the particles in pp collisions at 200 GeV. Various centrality bins for $\pi^+ + \pi^-$, $K^+ + K^-$, $p + \bar{p}$ and $\Lambda + \bar{\Lambda}$ are 0 – 5%, 0 – 10%, 10 – 20%, 20 – 40%, 40 – 60%, 60 – 80%, and 80 – 100%, and 0 – 10%, 10 – 20%, 20 – 40%, 40 – 60%, 60 – 80%, and 80 – 100% in panel (a)-(c) are scaled by 1/2, 1/4, 1/7, 1/10, 1/13 and 1/16 respectively. Panel (e) represents the p_T spectra of π^+ , π^- , K^+ , K^- , p , \bar{p} , ϕ and Ξ^- , and the spectra of p and \bar{p} , ϕ and Ξ^- are scaled by 2, 50 and 10 respectively.

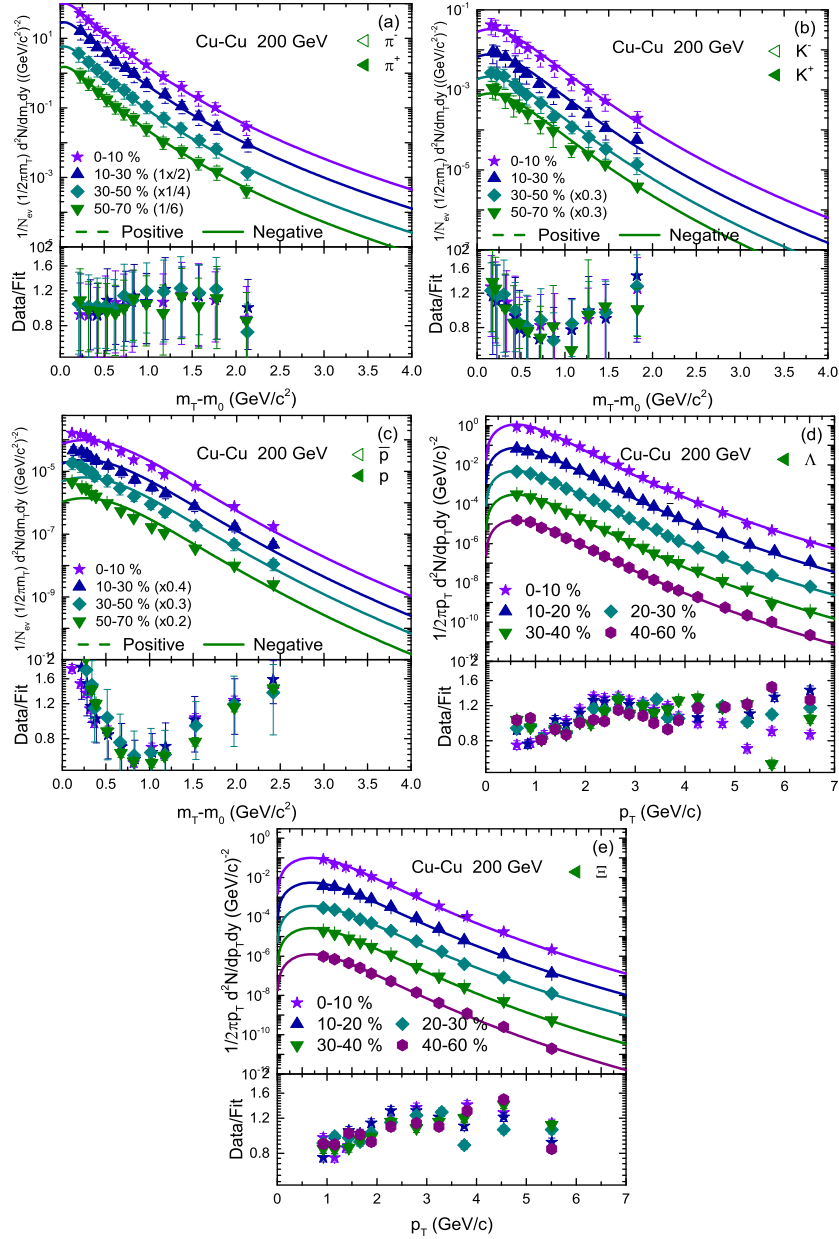


Fig. 1. The transverse momentum spectra of π^+ , π^- , K^+ , K^- , p , \bar{p} , Λ and Ξ in Copper-Copper (Cu-Cu) collisions at 200 GeV in various centrality classes. The experimental data of BRAHMS Collaboration at RHIC for π^+ , π^- , K^+ , K^- , p and \bar{p} is taken from ref. [47] at $|y| < 0$, while for Λ and Ξ is from ref. [48] at $|y| < 0.5$.

One can see that the modified Hagedorn function fits the experimental data well. The results of the data/fit ratio are given in figure followed by each panel. The data for $\pi^+ + \pi^-$, $K^+ + K^-$, $p + \bar{p}$ and $\Lambda + \bar{\Lambda}$ in panels (a-e) is taken from ref. [54], while the data for π^+ , π^- , K^+ , K^- , p , \bar{p} , and ϕ and Ξ^- are taken from ref. [55–57] respectively.

B. Tendencies of parameters

In order to study the tendency of parameters, the dependences of T_0 on centrality in (a)-(e) and T_0 on m_0 in (f) with different symbols are displayed in Figure 6. The values of the two parameters are cited from Table 1. Each panel represent the results from different collisions. The symbols in the figure are used in order to represent different particles. The parameters trend from left to right shows the behavior of T_0 from central to periph-

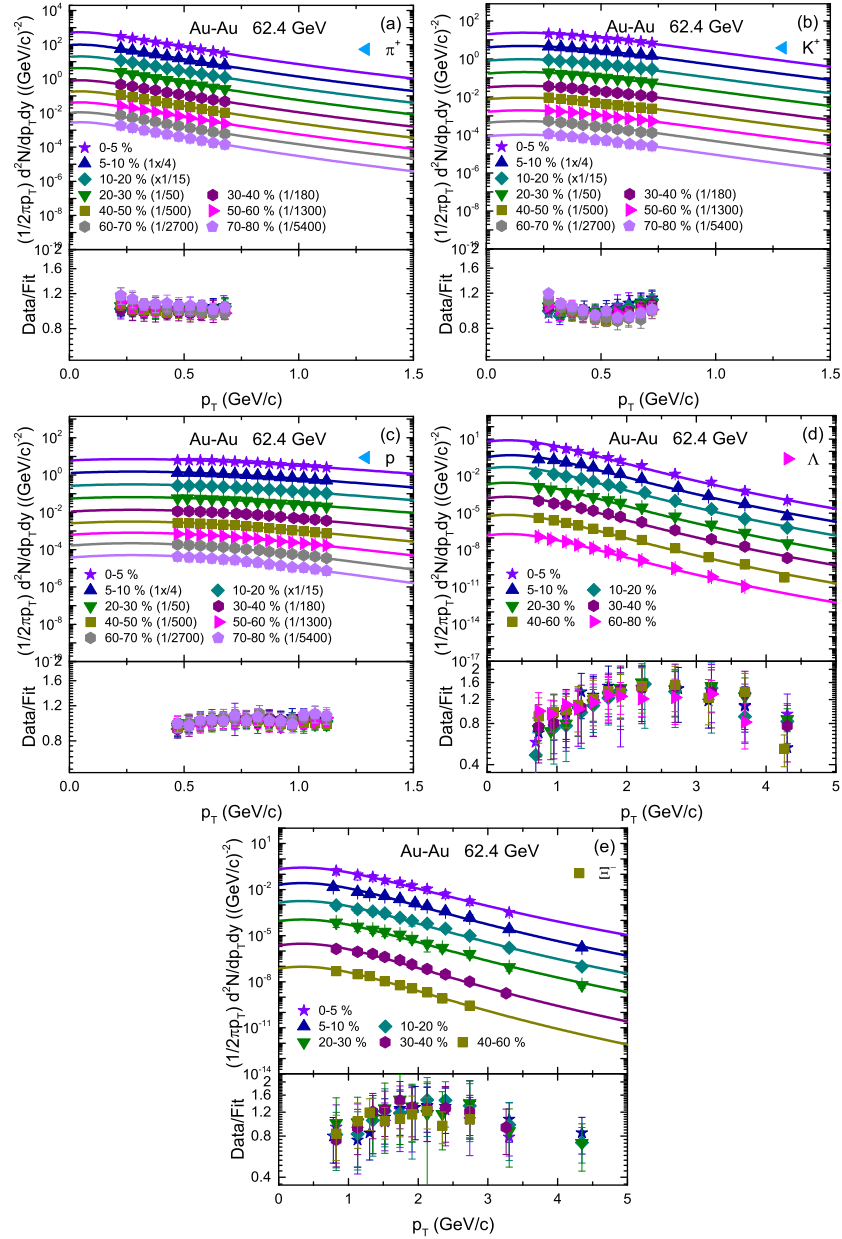


Fig. 2. The transverse momentum spectra of π^+ , K^+ , p , Λ and Ξ^- in Gold-Gold (Au-Au) collisions at 62.4 GeV in various centrality classes. The experimental data of STAR Collaboration at RHIC for π^+ , K^+ and p are taken from ref. [49] at $|\eta| < 0.1$ rapidity, while for Λ and Ξ is taken from ref. [50] at $|\eta| < 1.8$

eral collisions from panel (a)-(e) while panel (f) shows its behavior with increasing mass of the particle. In panels (a)-(e) one can see that T_0 for all the particles is larger in central collisions and it decrease as the centrality decrease due the reason that more energy is deposited to the system in central collisions due to the involvement of large number of participants which decrease towards periphery. In addition, from panel (a)-(f), T_0 is larger for the strange particles and the separate decoupling of the strange and non-strange particles is observed. The

larger T_0 for the strange particles is due to their smaller cross-section interaction, and according to kinematics, the reactions with lower cross-section is expected to be switched-off at higher temperatures/densities or early in time than the reactions with higher cross-sections. We also believe that the charm particles may decouple earlier than the strange particles and it is possible that a series of freeze-outs correspond to particular reaction channels [58], but it is a regret that we don't have the data for charm particles. Furthermore, one can see that T_0 is

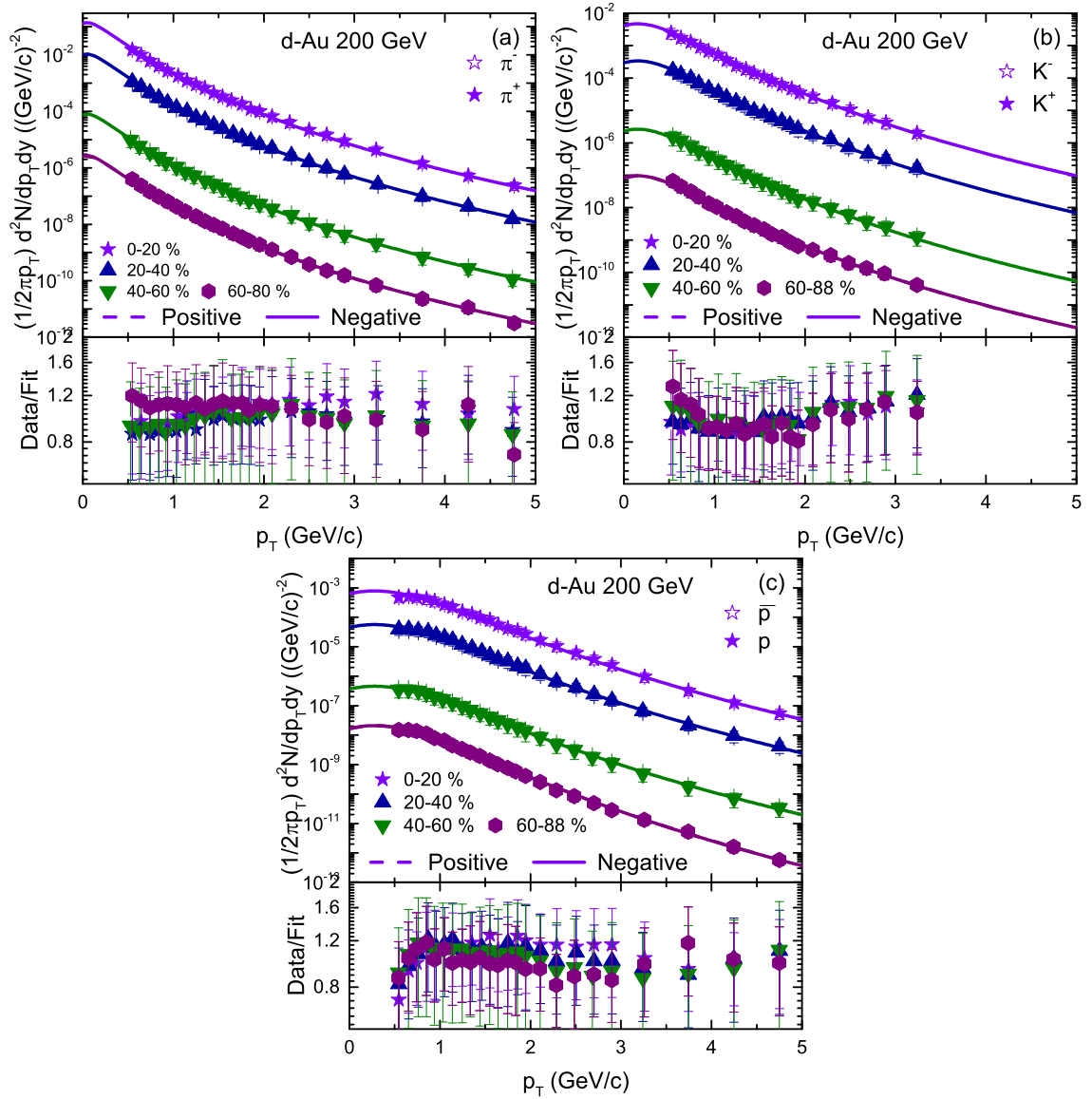


Fig. 3. The transverse momentum spectra of π^+ , π^- , K^+ , K^- , p and \bar{p} in Deuteron-Gold (d-Au) collisions at 200 GeV in various centrality intervals and the experimental data of PHENIX Collaboration at RHIC are taken from ref. [51] at $|\eta| < 0.35$.

larger at LHC than that of RHIC, and even at RHIC pp is the smallest collisions system and the observed T_0 in it is very smaller than the rest which is a clear evidence of T_0 on the size of the interacting system. From the above observation, one thing is clear that there is a strong dependence of T_0 on the collision energy because Pb-Pb and p-Pb collisions are the largest systems and they have larger T_0 , and pp is the smallest collision system among them and has smaller value for T_0 . However Cu-Cu, Au-Au and d-Au at RHIC, and p-Pb and Pb-Pb at LHC are different systems and have almost the same values for T_0 respectively, and this is due to the effect of collision energy. So we can conclude that T_0 is dependent

on the size of the collision system as well as the collision energy.

We would like to point out that we have observed two kinetic freeze-out scenarios which is agreement with [59], but in contrast with our recent work [60]. In fact, there are different freeze-out scenarios in literature which include one, two, three or multiple kinetic freeze-out scenarios. No doubt, the process of high energy collisions is complex and it is very interesting to see whether one, two, or multiple kinetic freeze-out scenarios exist in it. Due to the fact that different scenarios are reported in different literature, it is an open question up to now.

Fig. 7 shows similar to the fig. 6, but it shows the

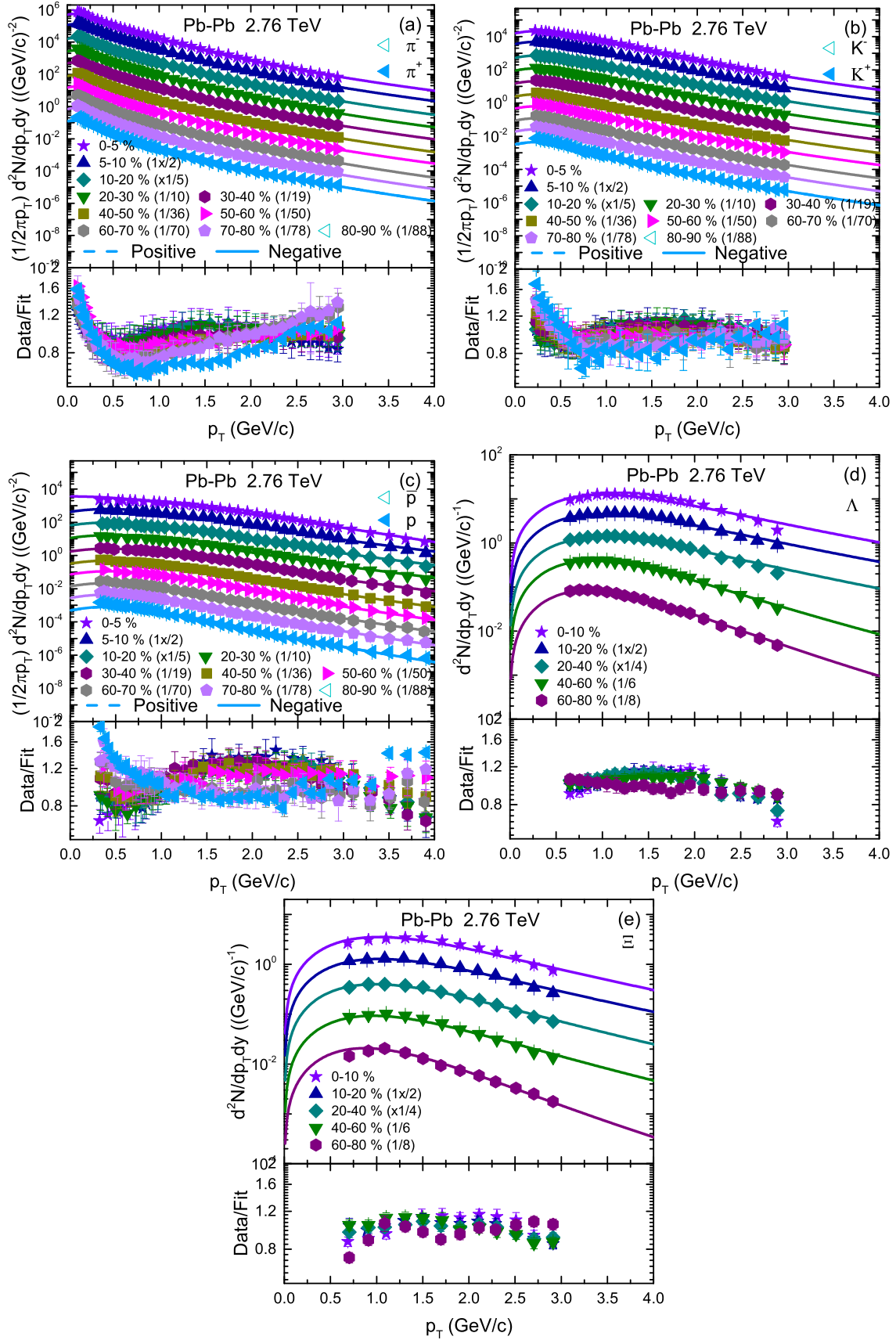


Fig. 4. The transverse momentum spectra of π^+ , π^- , K^+ , K^- , p , \bar{p} , Λ and Ξ^- in Lead-Lead (Pb-Pb) collisions at 2.76 TeV in various centrality classes. The experimental data of ALICE Collaboration at LHC for π^+ , π^- , K^+ , K^- , p and \bar{p} are from ref. [52] at $|y| < 0.5$ and for Λ and Ξ^- is taken from ref. [53] at $|y| < 0.5$ mid-rapidity.

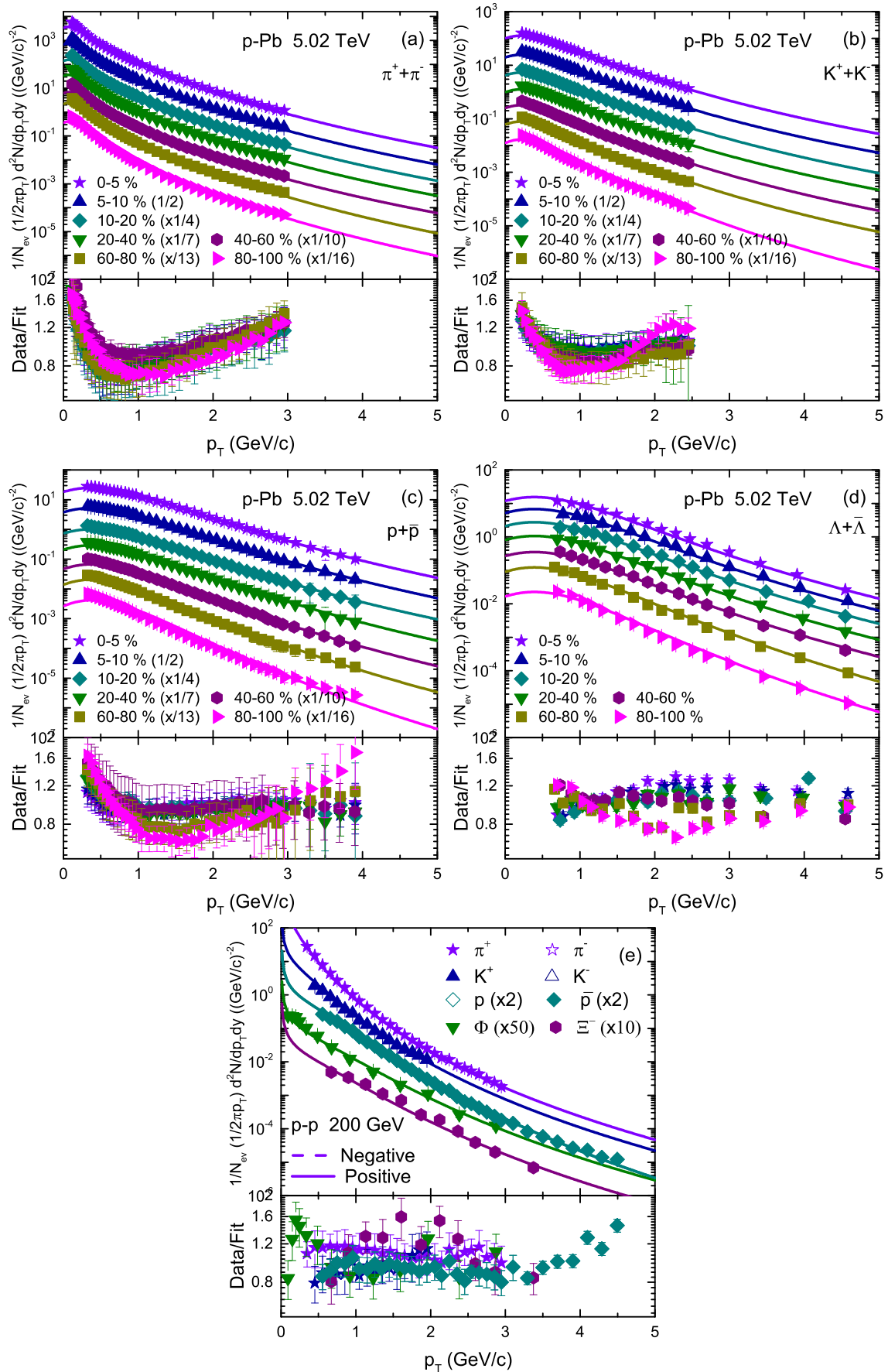


Fig. 5. Panel (a)-(d) show the transverse momentum spectra of $\pi^+ + \pi^-$, $K^+ + K^-$, $p + \bar{p}$ and $\Lambda + \bar{\Lambda}$ in Lead-Lead (Pb-Pb) collisions at 5.02 TeV in various centrality classes in p-Pb collisions, and panel (e) shows the transverse momentum spectra of π^+ , π^- , K^+ , K^- , p , \bar{p} , ϕ and Ξ^- in pp collisions at 200 GeV. The experimental data of BRAHMS Collaboration at LHC for $\pi^+ + \pi^-$, $K^+ + K^-$, $p + \bar{p}$ and $\Lambda + \bar{\Lambda}$ in panels (a-e) are taken from ref. [54] at mid-rapidity at $|y| < 0.5$, while the data for π^+ , π^- , K^+ , K^- , p , \bar{p} , and the data for ϕ and Ξ^- measured at STAR Collaboration are taken from ref. [56, 57] respectively at

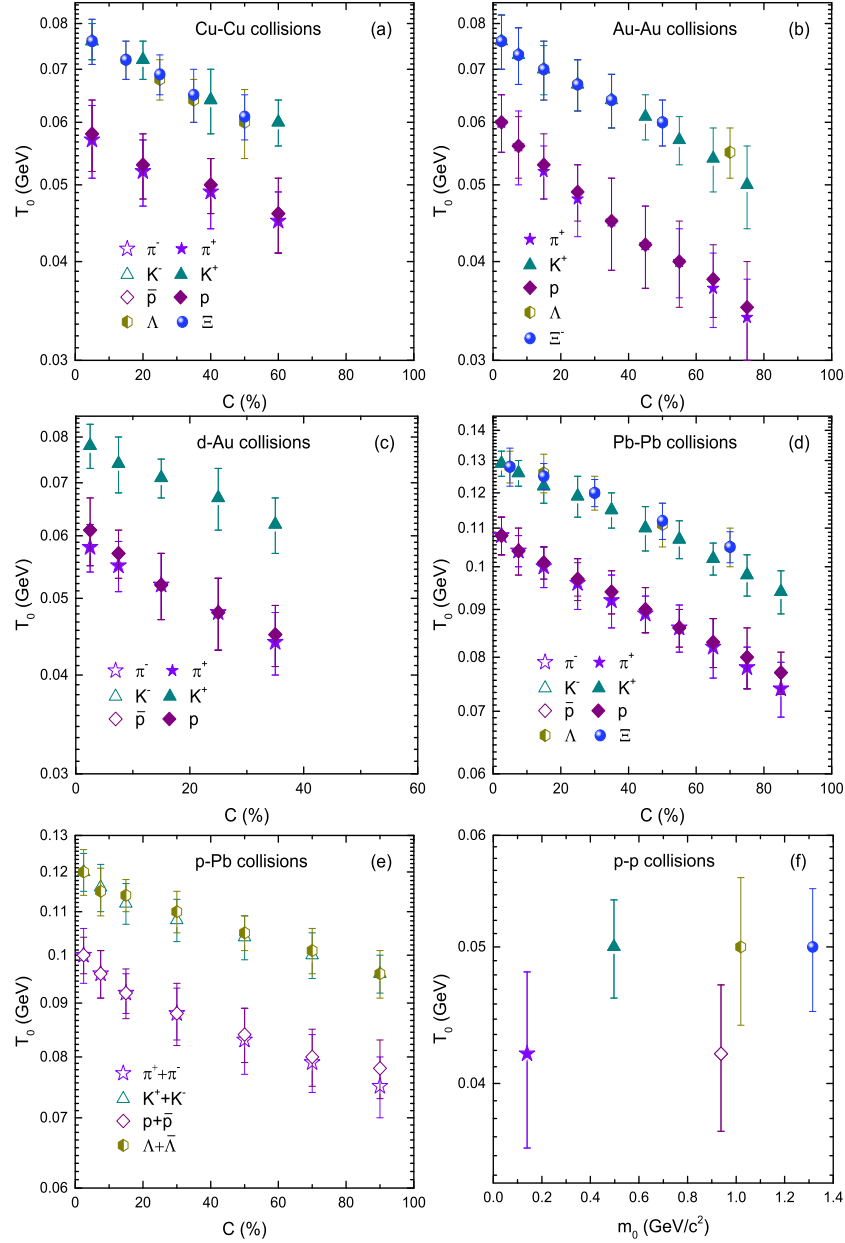


Fig. 6. Dependence of T_0 on centrality in panel (a)-(e), and dependence of T_0 on m_0 in panel (f).

dependence of β_T on centrality from panel (a)-(e), while panel (f) shows the dependence of β_T on m_0 . One can see that β_T remains invariant as we go from central to peripheral collision due to the reason that collective behavior from central to peripheral collisions does not change. In addition, β_T from panel (a)-(f) is larger for the lighter particles and it decreases for the heavier particles and it is a natural hydrodynamical behavior because heavier particles are left behind in the system. We also noticed that like T_0 , β_T in Cu-Cu, Au-Au and d-Au at RHIC, and Pb-Pb and p-Pb at LHC are close to each other due to the effect of their dependence on both the collision cross-

section and collision energy.

To check the dependence of V on centrality (mass), fig. 8 is represented. It is similar to that of fig. 6 and fig. 7. One can see that V decreases from central to peripheral collisions in panels (a)-(e) due to the fact that the participant nucleons decrease as we go from central to peripheral collisions depending on the interaction volume. The system which contains more participants reaches equilibrium quickly because there are a large number of secondary collisions by the re-scattering of partons in central collisions, and the system goes away from equilibrium states as it goes from central to peripheral collision

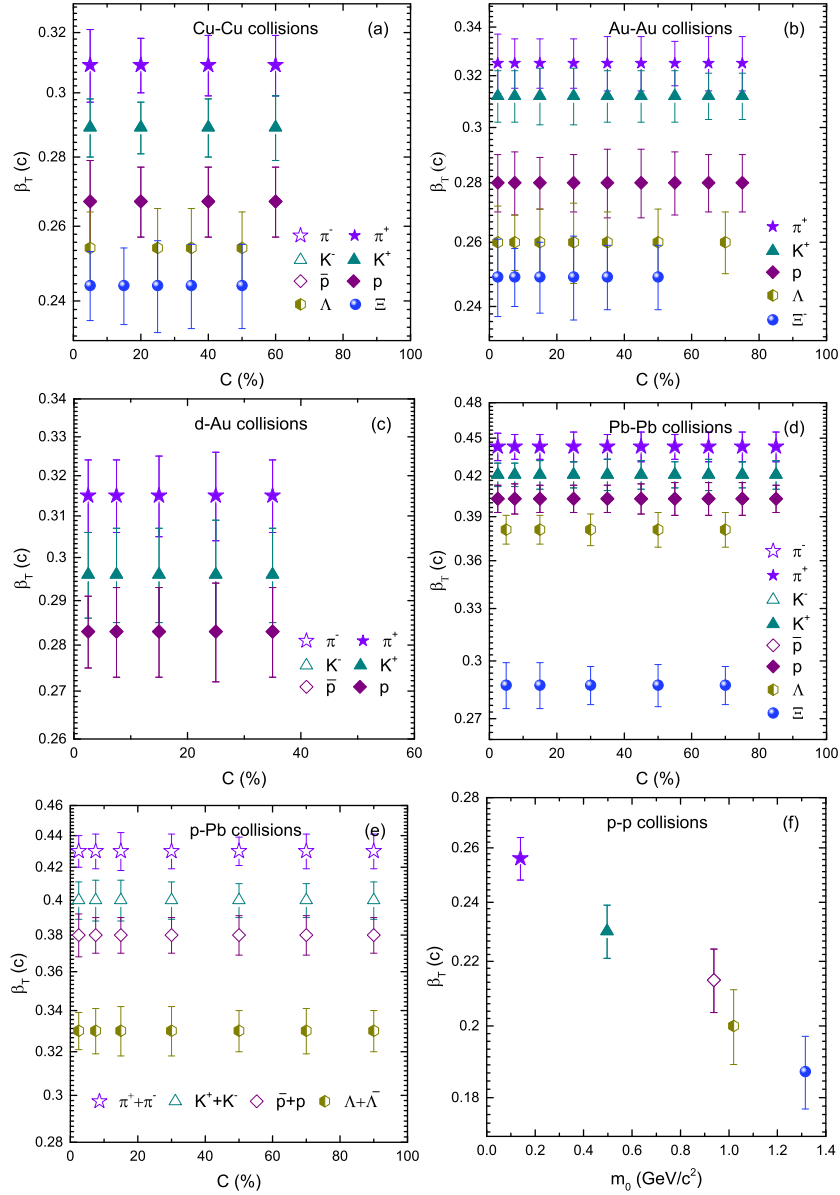


Fig. 7. Dependence of β_T on centrality in panel (a)-(e), and dependence of β_T on m_0 in panel (f).

due to reason that the number of participants in the system decreases. Furthermore, we observed that V from panel (a)-(f) is dependent of m_0 . Heavier the particle is, smaller is the value of V , which reveals a volume differential freeze-out scenario, and may indicate that there are different freeze-out surfaces for different particles. Like T_0 and β_T , V at LHC is larger than at RHIC and in pp collisions V is the smallest among all these systems, nucleus-nucleus collision systems at RHIC and LHC have nearly same V respectively and this is due to their energy difference.

Fig. 9 represents the behavior of the parameter n . $n=1/(q-1)$, and q is the entropy index, which is re-

ferred to equilibrium degree. In general, $q=1$ corresponds to equilibrium state, where $q>1$ corresponds to non-equilibrium state. Smaller q corresponds to large n . One can see that the parameter n is larger in almost all the cases which means that the system is in equilibrium state, and also it remains constant in most cases from central to peripheral collision except for proton that increases from central to peripheral collisions which is not understood by us.

The dependence of the parameter N_0 on centrality (m_0). N_0 is a normalization constant but it has its significance too. It reflects the multiplicity. One can see that the parameter N_0 decreases from central to peripheral

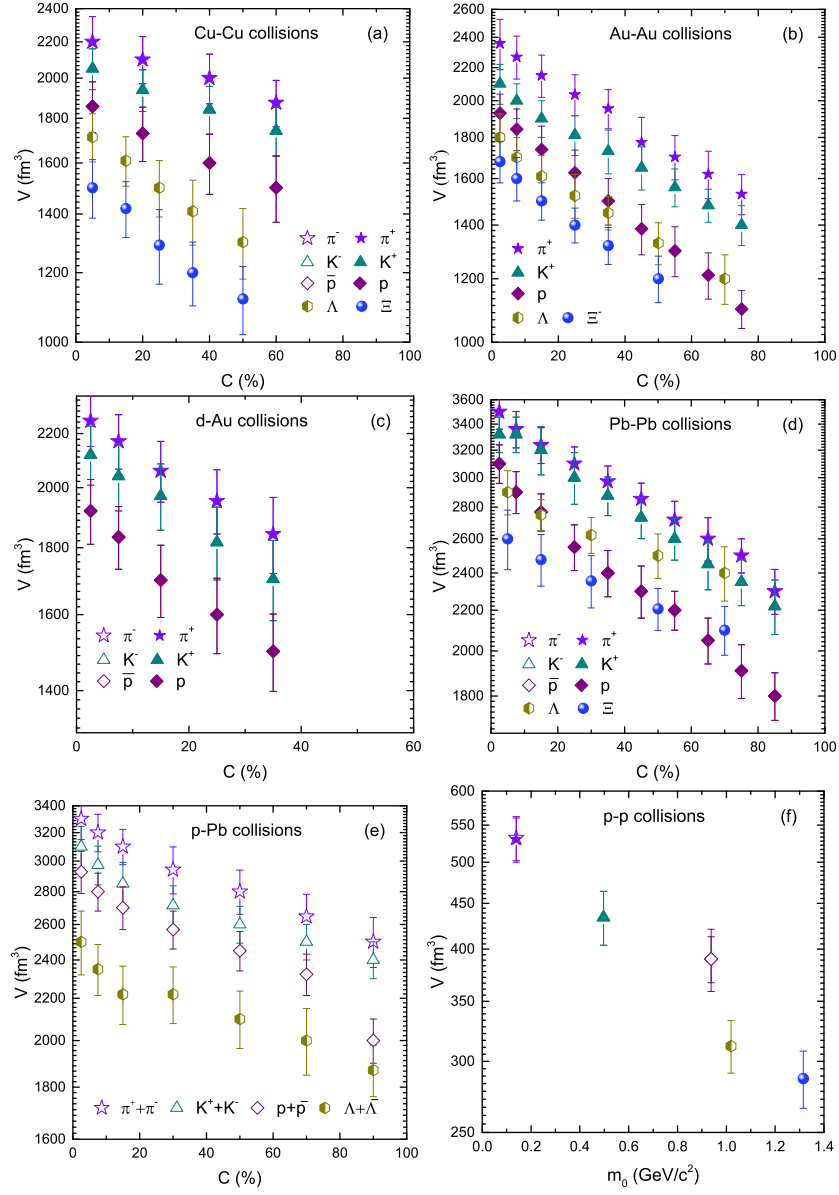


Fig. 8. Dependence of V on centrality in panel (a)-(e), and dependence of V on m_0 in panel (f).

collisions which indicates that the multiplicity decreases as the system goes from central to peripheral collisions. It can also be seen that N_0 is dependent on the size of the interacting system. As we can see that in Au-Au collisions it is larger than Cu-Cu and d-Au collisions, and in Pb-Pb collisions it has the highest value followed by p-Pb collisions. In pp collisions N_0 is the smallest due to being it is the smallest system among them. This shows that the multiplicity depends on the size of the interacting system and also have the collision energy dependence as the collision energy of the AA collisions at RHIC and LHC are different.

The mean transverse momentum ($\langle p_T \rangle$) depen-

dence on centrality (m_0) is demonstrated in fig. 11. One can see that $\langle p_T \rangle$ decrease as the system goes from central to peripheral collisions and this is due to the fact that the system gains large momentum (energy) in central collisions where further multiple scattering happens, which decrease when the system goes towards periphery. Like T_0 and β_T , $\langle p_T \rangle$ also depends on the size of the interacting system and also there is an effect on the behavior of collision energy. We also analyze root-mean-square p_T ($\sqrt{\langle p_T^2 \rangle}$) over $\sqrt{2}$ ($\sqrt{\langle p_T^2 \rangle}/\sqrt{2}$) in fig. 12. and showed its behavior with changing the centrality (m_0). ($\sqrt{\langle p_T^2 \rangle}/\sqrt{2}$) represents the initial temperature (T_i) of the interacting system according to the string per-

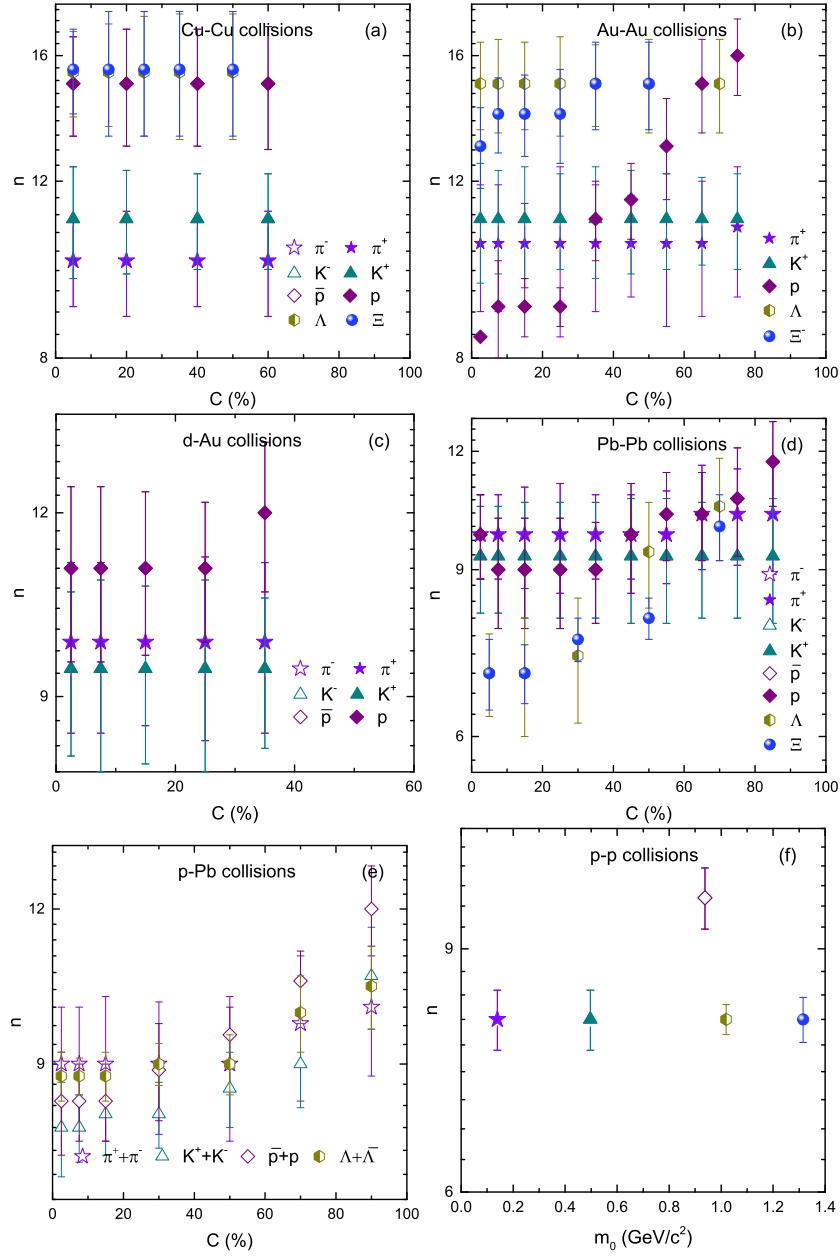


Fig. 9. Dependence of n on centrality in panel (a)-(e), and dependence of n on m_0 in panel (f).

colation model [61–63]. It can be obviously seen that the initial temperature is larger in central collisions, however it decrease from central to peripheral collision systems, and similar to T_0 it depends on the size of the interacting system and is also effected by the collision energy. Moreover, we have observed that the initial temperature depends on mass of the particle. The more massive the particle is, the larger is the initial temperature.

We would like to point out that the initial temperature depends on mass of the particle, and the more heavier the particle is, the larger the initial temperature, how-

ever the kinetic freeze-out temperature depends on the cross-section interaction of the particles. The larger the cross-section of the particle is, the smaller the value of kinetic freeze-out temperature. The difference in the two temperatures is due to the reason that they occur at two different process in the system evolution. Furthermore, it is also possible that the centrality dependence of the two types of temperatures is also different if one gets the increasing trend from central to peripheral for T_0 which is observed in our recent work [64, 65]. In fact the trend dependence of T_0 is also an open question in high energy

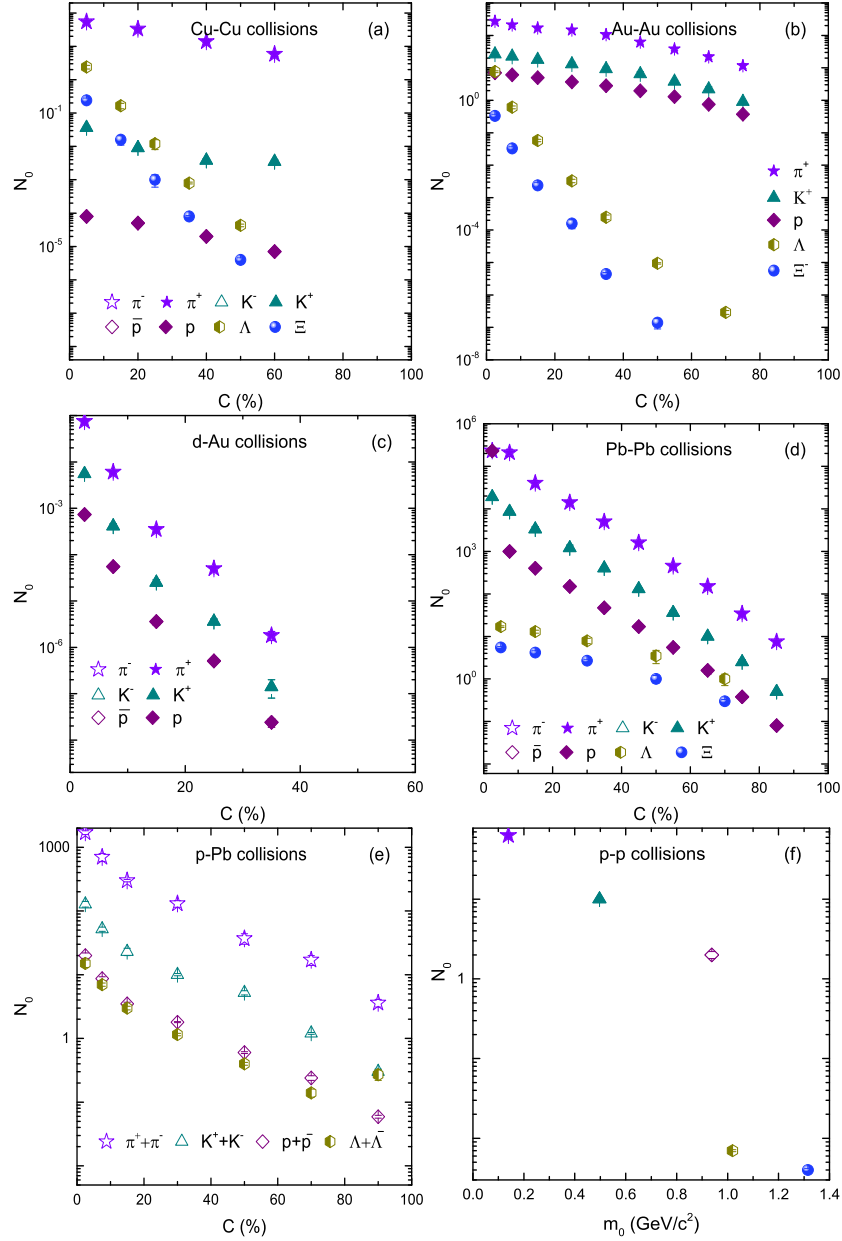


Fig. 10. Dependence of N_0 on centrality in panel (a)-(e), and dependence of N_0 on m_0 in panel (f).

collisions because different literature give different trend.

Before going to the summary and conclusions, we would like to point out that the initial temperature is observed to be larger than the kinetic freeze-out temperature. The former is followed by the chemical freeze-out temperature which can be expressed as

$$T_{ch} = \frac{T_{lim}}{1 + \exp[2.60 - \ln(\sqrt{s_{NN}})/0.45]} \quad (4)$$

where $T_{lim}=0.1584$ GeV. The chemical freeze-out temperature is followed by the effective temperature and then the kinetic freeze-out temperature and this order

is in agreement with the order of time evolution of the interacting system.

IV. SUMMARY AND CONCLUSIONS

We summarize here our main observations and conclusions.

(a) The transverse momentum spectra of strange and non-strange hadrons produced in Cu-Cu, Au-Au, d-Au, Pb-Pb, p-Pb and pp collisions have been studied by the modified Hagedorn model. The results are well in

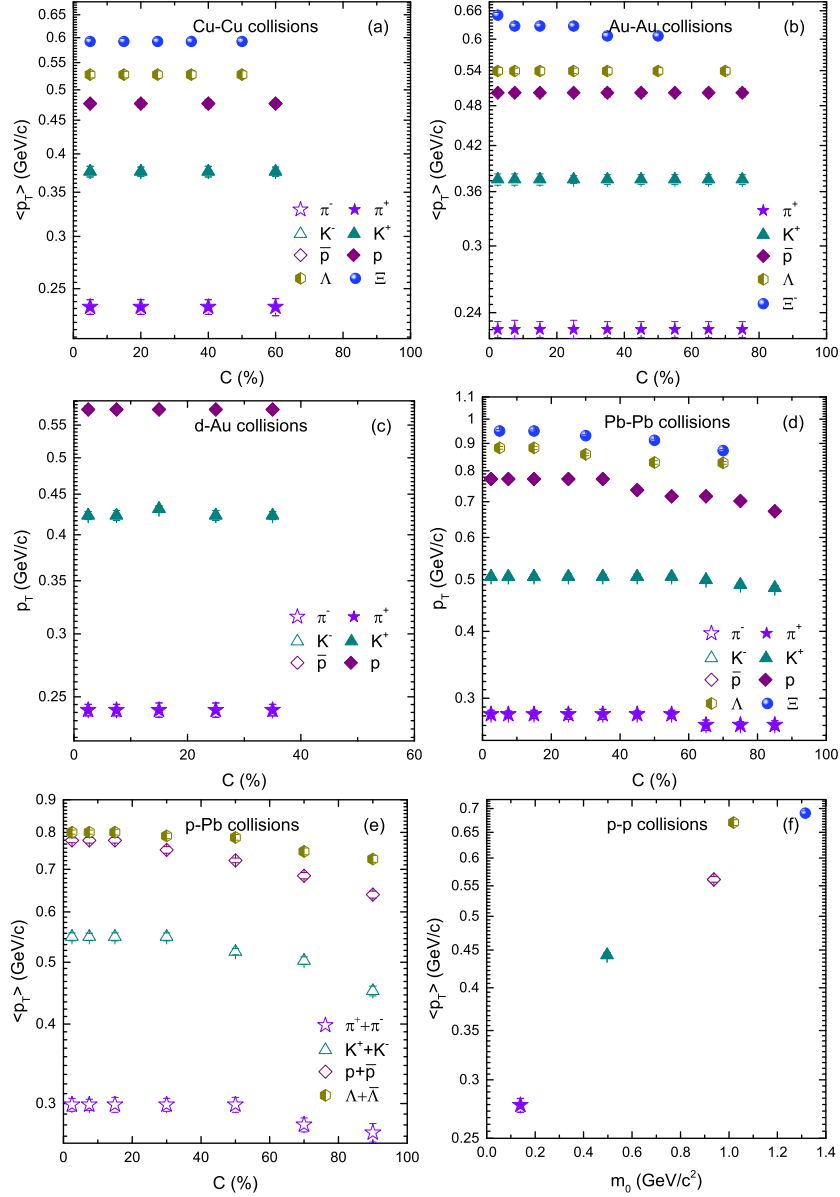


Fig. 11. Dependence of $\langle p_T \rangle$ on centrality in panel (a)-(e), and dependence of $\langle p_T \rangle$ on m_0 in panel (f).

agreement with the experimental data BRAHM, STAR, PHENIX and ALICE Collaborations at RHIC and LHC.

(b) T_0 and T_i are larger in central collisions and they decrease from central to peripheral collisions due to the decrease in the participant nucleons towards periphery which results in lower degree of excitation of the system in the peripheral collisions. $\langle p_T \rangle$ also decrease towards periphery due to the reason that the energy (momentum) transfer becomes lower in the system from central to peripheral collisions. In addition V is larger in central collisions and it decrease towards periphery due to the reason of decreasing of partons re-scattering towards periphery.

(c) β_T depends on the mass of the particle. Heavier

the particle is, smaller is the value of β_T is. β_T remains unchanged from central to peripheral collisions because the collective flow from central to peripheral collisions does not change.

(d) The parameter N_0 represents the multiplicity and it decrease from central to peripheral collisions.

(e) T_0 depends on the cross-section interaction of the particle and therefore the strange and non-strange particles have separate freeze-out and it reveals the scenario of two kinetic freeze-out temperature, while the initial temperature depends on the mass of the particle and this is due to the reason that both of them occurs at different stages in the evolution system.

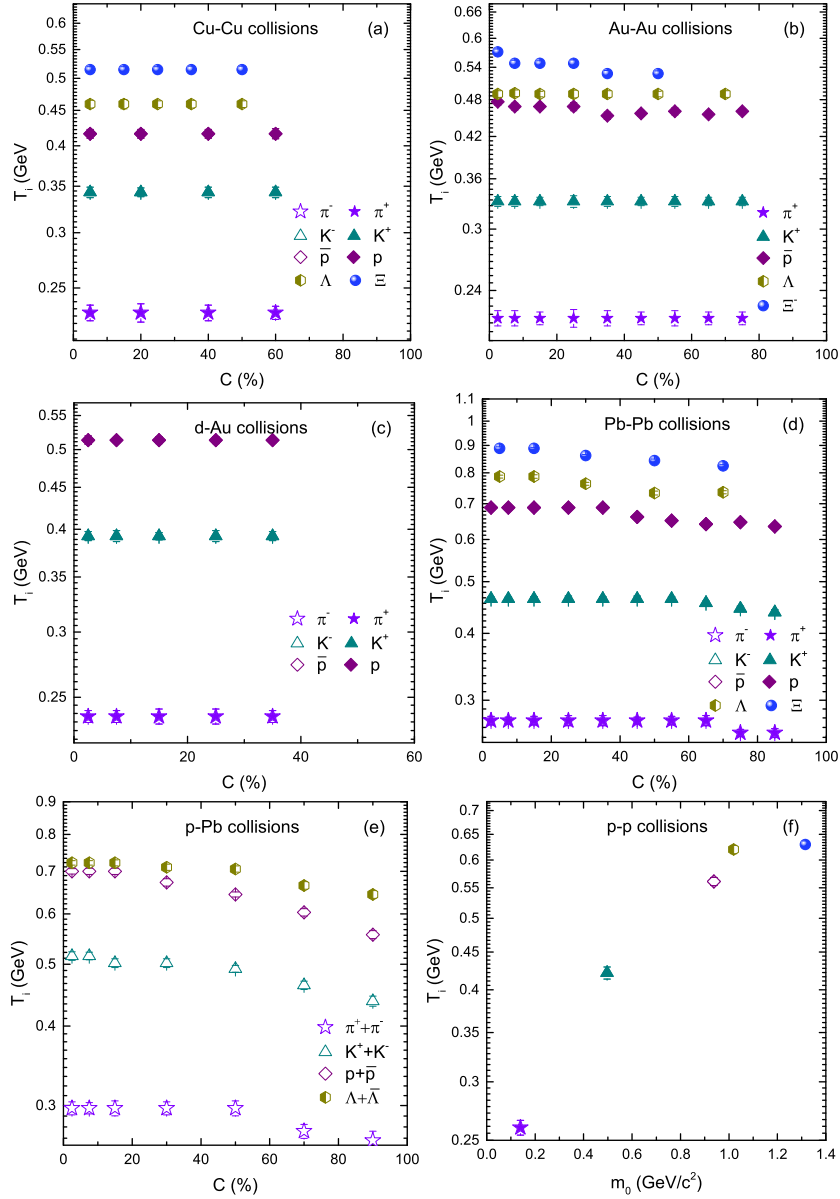


Fig. 12. Dependence of T_i on centrality in panel (a)-(e), and dependence of T_i on m_0 in panel (f).

(f) V depends on the mass of the particle. The heavier particle has smaller V which reveals the volume differential freeze-out scenario and indicates a separate freeze-out surface for each particle.

(g) T_0 , T_i , β_T , V , $\langle p_T \rangle$ and N_0 are dependent on the size of the interacting system because all these parameters have larger values at LHC collision systems than at RHIC collision systems and in pp collisions it has the lowest values. The mentioned parameters in Cu-Cu, d-Au, and Au-Au are different collision systems with different energies (200 GeV, 62.4 GeV and 200 GeV for Cu-Cu, Au-Au and d-Au respectively), but the values of the parameters observed in these systems are nearly

equal, due to their dependence on both the collision energy and collision cross-section. Similar behavior is observed in p-Pb and Pb-Pb collisions.

Acknowledgments

This research was funded by the National Natural Science Foundation of China grant number 11875052, 11575190, and 11135011.

Author Contributions All authors listed have made a substantial, direct, and intellectual contribution to the work and approved it for publication.

Data Availability Statement This manuscript has no associated data or the data will not be deposited. [Authors' comment: The data used to support the findings of this study are included within the article and are cited at relevant places within the text as references.]

Compliance with Ethical Standards

Ethical Approval The authors declare that they are in compliance with ethical standards regarding the content of this paper.

Disclosure The funding agencies have no role in the design of the study; in the collection, analysis, or interpretation of the data; in the writing of the manuscript, or in the decision to publish the results.

Conflict of Interest The authors declare that there are no conflicts of interest regarding the publication of this paper.

-
- [1] U. W. Heinz, “Concepts of heavy ion physics,” [arXiv:hep-ph/0407360 [hep-ph]].
 - [2] P. Braun-Munzinger and J. Wambach, “The Phase Diagram of Strongly-Interacting Matter,” *Rev. Mod. Phys.* **81**, 1031-1050 (2009) doi:10.1103/RevModPhys.81.1031 [arXiv:0801.4256 [hep-ph]].
 - [3] W. Florkowski, “Basic phenomenology for relativistic heavy-ion collisions,” *Acta Phys. Polon. B* **45**, no.12, 2329-2354 (2014) doi:10.5506/APhysPolB.45.2329 [arXiv:1410.7904 [nucl-th]].
 - [4] F. A. Flor, G. Olinger and R. Bellwied, “System Size and Flavour Dependence of Chemical Freeze-out Temperatures in ALICE pp , pPb and $PbPb$ Collisions at LHC Energies,” [arXiv:2109.09843 [nucl-ex]].
 - [5] H. Liu [STAR], “Light Nuclei Production in Au+Au Collisions at $\sqrt{s_{NN}} = 3$ GeV from the STAR experiment,” [arXiv:2110.10929 [nucl-ex]].
 - [6] A. A. Akhondov, Y. Ali, M. Q. Haseeb and M. K. Suleymanov, “Study of Strange Particle Production in Central Pb-Pb Collisions at $\sqrt{s} = 2.76$ TeV,” *Journal of Physics & Optics Sciences* **2**, no.4, 1-6 (2021)
 - [7] R. N. Patra, B. Mohanty and T. K. Nayak, “Centrality, transverse momentum and collision energy dependence of the Tsallis parameters in relativistic heavy-ion collisions,” *Eur. Phys. J. Plus* **136**, no.6, 702 (2021) doi:10.1140/epjp/s13360-021-01660-0 [arXiv:2008.02559 [hep-ph]].
 - [8] J. Adam *et al.* [STAR], “Centrality and transverse momentum dependence of D^0 -meson production at mid-rapidity in Au+Au collisions at $\sqrt{s_{NN}} = 200$ GeV,” *Phys. Rev. C* **99**, no.3, 034908 (2019) doi:10.1103/PhysRevC.99.034908 [arXiv:1812.10224 [nucl-ex]].
 - [9] U. W. Heinz, “Strange messages: Chemical and thermal freezeout in nuclear collisions,” *J. Phys. G* **25**, 263-274 (1999) doi:10.1088/0954-3899/25/2/014 [arXiv:nucl-th/9810056 [nucl-th]].
 - [10] S. Chatterjee, R. M. Godbole and S. Gupta, “Strange freezeout,” *Phys. Lett. B* **727**, 554-557 (2013) doi:10.1016/j.physletb.2013.11.008 [arXiv:1306.2006 [nucl-th]].
 - [11] M. Waqas, G. X. Peng, F. H. Liu and Z. Wazir, “Effects of coalescence and isospin symmetry on the freeze-out of light nuclei and their anti-particles,” *Sci. Rep.* **11**, no.1, 20252 (2021) doi:10.1038/s41598-021-99455-x [arXiv:2105.01300 [hep-ph]].
 - [12] M. Waqas, G. X. Peng and F. H. Liu, “An evidence of triple kinetic freezeout scenario observed in all centrality intervals in Cu–Cu, Au–Au and Pb–Pb collisions at high energies,” *J. Phys. G* **48**, no.7, 075108 (2021) doi:10.1088/1361-6471/abdd8d [arXiv:2101.07971 [hep-ph]].
 - [13] M. Waqas, F. H. Liu and Z. Wazir, “Dependence of temperatures and kinetic freeze-out volume on centrality in Au–Au and Pb–Pb collisions at high energy,” *Adv. High Energy Phys.* **2020**, 8198126 (2020) doi:10.1155/2020/8198126 [arXiv:2004.03773 [hep-ph]].
 - [14] M. Waqas and F. H. Liu, “Initial, effective, and kinetic freeze-out temperatures from transverse momentum spectra in high-energy proton(deuteron)–nucleus and nucleus–nucleus collisions,” *Eur. Phys. J. Plus* **135**, no.2, 147 (2020) doi:10.1140/epjp/s13360-020-00213-1 [arXiv:1911.01709 [hep-ph]].
 - [15] S. Chatrchyan *et al.* [CMS], “Study of high- p_T charged particle suppression in PbPb compared to pp collisions at $\sqrt{s_{NN}} = 2.76$ TeV,” *Eur. Phys. J. C* **72**, 1945 (2012) doi:10.1140/epjc/s10052-012-1945-x [arXiv:1202.2554 [nucl-ex]].
 - [16] M. Suleymanov, “The meaning behind observed p_T regions at the LHC energies,” *Int. J. Mod. Phys. E* **27**, no.01, 1850008 (2018) doi:10.1142/S0218301318500088 [arXiv:1707.03420 [nucl-ex]].
 - [17] M. Waqas and F. H. Liu, “Centrality dependence of kinetic freeze-out temperature and transverse flow velocity in high energy nuclear collisions,” doi:10.1007/s12648-021-02058-5 [arXiv:1806.05863 [hep-ph]].

- [18] M. Waqas and G. X. Peng, “Study of Dependence of Kinetic Freezeout Temperature on the Production Cross-Section of Particles in Various Centrality Intervals in Au–Au and Pb–Pb Collisions at High Energies,” *Entropy* **23**, 488 (2021) doi:10.3390/e23040488 [arXiv:2104.12067 [hep-ph]].
- [19] E. Schnedermann, J. Sollfrank and U. W. Heinz, “Thermal phenomenology of hadrons from 200-A/GeV S+S collisions,” *Phys. Rev. C* **48**, 2462-2475 (1993) doi:10.1103/PhysRevC.48.2462 [arXiv:nucl-th/9307020 [nucl-th]].
- [20] B. I. Abelev *et al.* [STAR], “Systematic Measurements of Identified Particle Spectra in pp, d^+ Au and Au+Au Collisions from STAR,” *Phys. Rev. C* **79**, 034909 (2009) doi:10.1103/PhysRevC.79.034909 [arXiv:0808.2041 [nucl-ex]].
- [21] K. Jiang, Y. Zhu, W. Liu, H. Chen, C. Li, L. Ruan, Z. Tang, Z. Xu and Z. Xu, “Onset of radial flow in p+p collisions,” *Phys. Rev. C* **91**, no.2, 024910 (2015) doi:10.1103/PhysRevC.91.024910 [arXiv:1312.4230 [nucl-ex]].
- [22] J. Chen, J. Deng, Z. Tang, Z. Xu and L. Yi, “Nonequilibrium kinetic freeze-out properties in relativistic heavy ion collisions from energies employed at the RHIC beam energy scan to those available at the LHC,” *Phys. Rev. C* **104**, no.3, 034901 (2021) doi:10.1103/PhysRevC.104.034901 [arXiv:2012.02986 [nucl-th]].
- [23] Z. Tang, Y. Xu, L. Ruan, G. van Buren, F. Wang and Z. Xu, “Spectra and radial flow at RHIC with Tsallis statistics in a Blast-Wave description,” *Phys. Rev. C* **79**, 051901 (2009) doi:10.1103/PhysRevC.79.051901 [arXiv:0812.1609 [nucl-ex]].
- [24] M. Waqas, F. H. Liu, R. Q. Wang and I. Siddique, *Eur. Phys. J. A* **56**, no.7, 188 (2020) doi:10.1140/epja/s10050-020-00192-y [arXiv:2007.00825 [hep-ph]].
- [25] J. Q. Tao, M. Wang, H. Zheng, W. C. Zhang, L. L. Zhu and A. Bonasera, “Pseudorapidity distributions of charged particles in pp , p(d)A and AA collisions using Tsallis thermodynamics,” *J. Phys. G* **48**, no.10, 105102 (2021) doi:10.1088/1361-6471/ac1393 [arXiv:2011.05026 [nucl-th]].
- [26] G. R. Che, J. B. Gu, W. C. Zhang and H. Zheng, *J. Phys. G* **48**, 095103 (2021) doi:10.1088/1361-6471/ac09dc [arXiv:2010.14880 [nucl-th]].
- [27] M. Ajaz, A. A. K. H. Ismail, A. Ahmed, Z. Wazir, R. Shehzadi, H. Younis, G. Khan, R. Khan, S. Ali and M. Waqas, *et al. Results Phys.* **30**, 104790 (2021) doi:10.1016/j.rinp.2021.104790
- [28] W. J. Xie, “Transverse momentum spectra in high-energy nucleus-nucleus, proton-nucleus and proton-proton collisions,” *Chin. Phys. C* **35**, 1111-1119 (2011) doi:10.1088/1674-1137/35/12/006
- [29] L. N. Gao, F. H. Liu and R. A. Lacey, “Excitation functions of parameters in Erlang distribution, Schwinger mechanism, and Tsallis statistics in RHIC BES program,” *Eur. Phys. J. A* **52**, no.5, 137 (2016) doi:10.1140/epja/i2016-16137-7 [arXiv:1604.07218 [hep-ph]].
- [30] L. N. Gao and F. H. Liu, “Comparing Erlang distribution and Schwinger mechanism on transverse momentum spectra in high energy collisions,” *Adv. High Energy Phys.* **2016**, 1505823 (2016) doi:10.1155/2016/1505823 [arXiv:1510.03520 [hep-ph]].
- [31] S. Tahery, X. Chen and L. Zou, “A comparison of condensate mass of QCD vacuum between Wilson line approach and Schwinger effect,” *Chin. Phys. C* **45**, no.4, 043107 (2021) doi:10.1088/1674-1137/abe03b [arXiv:2007.01559 [hep-th]].
- [32] R. C. Wang and C. Y. Wong, “Finite Size Effect in the Schwinger Particle Production Mechanism,” *Phys. Rev. D* **38**, 348-359 (1988) doi:10.1103/PhysRevD.38.348
- [33] H. Taya, “Dynamically assisted Schwinger mechanism and chirality production in parallel electromagnetic field,” *Phys. Rev. Res.* **2**, no.2, 023257 (2020) doi:10.1103/PhysRevResearch.2.023257 [arXiv:2003.08948 [hep-ph]].
- [34] H. Taya, “Mutual assistance between the Schwinger mechanism and the dynamical Casimir effect,” *Phys. Rev. Res.* **2**, no.2, 023346 (2020) doi:10.1103/PhysRevResearch.2.023346 [arXiv:2003.12061 [hep-ph]].
- [35] R. Hagedorn, “Multiplicities, p_T distributions and the expected hadron to quark-gluon phase transition,” *Riv. Nuovo Cimento* **6**(10), 1 (1983).
- [36] L. L. Li, F. H. Liu, M. Waqas, R. Al-Yusufi and A. Mujeer, *Adv. High Energy Phys.* **2020**, 5356705 (2020) doi:10.1155/2020/5356705 [arXiv:1911.07419 [hep-ph]].
- [37] J. Mashford, “Quantum chromodynamics through the geometry of Möbius structures,” [arXiv:1809.04457 [physics.gen-ph]].
- [38] N. A. Abdulov, A. V. Lipatov and M. A. Malyshev, “Inclusive Higgs Boson Production at the LHC within the QCD k_t -Factorization Approach,” *Phys. Atom. Nucl.* **82**, no.12, 1602-1606 (2020) doi:10.1134/S1063778819120019
- [39] M. Mieskolainen, “Combinatorial Superstatistics for Soft QCD,” [arXiv:1910.06279 [hep-ph]].
- [40] K. Aamodt *et al.* [ALICE], “Transverse momentum spectra of charged particles in proton-proton collisions at $\sqrt{s} = 900$ GeV with ALICE at the LHC,” *Phys. Lett. B* **693**, 53-68 (2010) doi:10.1016/j.physletb.2010.08.026 [arXiv:1007.0719 [hep-ex]].
- [41] B. Abelev *et al.* [ALICE], “Inclusive J/ψ production in pp collisions at $\sqrt{s} = 2.76$ TeV,” *Phys. Lett. B* **718**, 295-306 (2012) [erratum: *Phys. Lett. B* **748**, 472-473 (2015)] doi:10.1016/j.physletb.2012.10.078 [arXiv:1203.3641 [hep-ex]].
- [42] I. Lakomov [ALICE], “Event activity dependence of inclusive J/ψ production in p-Pb collisions at $\sqrt{s_{NN}} = 5.02$ TeV with ALICE at the LHC,” *Nucl. Phys. A* **931**,

- 1179-1183 (2014) doi:10.1016/j.nuclphysa.2014.08.062 [arXiv:1408.0702 [hep-ex]].
- [43] B. Abelev *et al.* [ALICE], “Light vector meson production in pp collisions at $\sqrt{s} = 7$ TeV,” *Phys. Lett. B* **710**, 557-568 (2012) doi:10.1016/j.physletb.2012.03.038 [arXiv:1112.2222 [nucl-ex]].
- [44] A. De Falco [ALICE], “Vector meson production in pp collisions at $\sqrt{s} = 7$ TeV, measured with the ALICE detector,” *J. Phys. G* **38**, 124083 (2011) doi:10.1088/0954-3899/38/12/124083 [arXiv:1106.4140 [nucl-ex]].
- [45] I. Abt *et al.* [HERA-B], “ K^0 and ϕ meson production in proton-nucleus interactions at $s^{*}(1/2) = 41.6$ -GeV,” *Eur. Phys. J. C* **50**, 315-328 (2007) doi:10.1140/epjc/s10052-007-0237-3 [arXiv:hep-ex/0606049 [hep-ex]].
- [46] K. K. Olimov, F. H. Liu, K. A. Musaev and M. Z. Shodmonov, “Analysis of multiplicity dependencies of midrapidity p_T distributions of identified charged particles in p+p collisions at $\sqrt{s}=7$ TeV at the LHC,” [arXiv:2109.00203 [hep-ph]].
- [47] I. C. Arsene *et al.* [BRAHMS], “Rapidity and centrality dependence of particle production for identified hadrons in Cu+Cu collisions at $\sqrt{s_{NN}} = 200$ GeV,” *Phys. Rev. C* **94**, no.1, 014907 (2016) doi:10.1103/PhysRevC.94.014907 [arXiv:1602.01183 [nucl-ex]].
- [48] G. Agakishiev *et al.* [STAR], “Strangeness Enhancement in Cu+Cu and Au+Au Collisions at $\sqrt{s_{NN}} = 200$ GeV,” *Phys. Rev. Lett.* **108**, 072301 (2012) doi:10.1103/PhysRevLett.108.072301 [arXiv:1107.2955 [nucl-ex]].
- [49] B. I. Abelev *et al.* [STAR], “Systematic Measurements of Identified Particle Spectra in pp, d^+ Au and Au+Au Collisions from STAR,” *Phys. Rev. C* **79**, 034909 (2009) doi:10.1103/PhysRevC.79.034909 [arXiv:0808.2041 [nucl-ex]].
- [50] M. M. Aggarwal *et al.* [STAR], “Strange and Multi-strange Particle Production in Au+Au Collisions at $\sqrt{s_{NN}} = 62.4$ GeV,” *Phys. Rev. C* **83**, 024901 (2011) doi:10.1103/PhysRevC.83.024901 [arXiv:1010.0142 [nucl-ex]].
- [51] A. Adare *et al.* [PHENIX], “Spectra and ratios of identified particles in Au+Au and d +Au collisions at $\sqrt{s_{NN}} = 200$ GeV,” *Phys. Rev. C* **88**, no.2, 024906 (2013) doi:10.1103/PhysRevC.88.024906 [arXiv:1304.3410 [nucl-ex]].
- [52] B. Abelev *et al.* [ALICE], “Centrality dependence of π , K , p production in Pb-Pb collisions at $\sqrt{s_{NN}} = 2.76$ TeV,” *Phys. Rev. C* **88**, 044910 (2013) doi:10.1103/PhysRevC.88.044910 [arXiv:1303.0737 [hep-ex]].
- [53] V. Begun, W. Florkowski and M. Rybczynski, “Transverse-momentum spectra of strange particles produced in Pb+Pb collisions at $\sqrt{s_{NN}} = 2.76$ TeV in the chemical non-equilibrium model,” *Phys. Rev. C* **90**, no.5, 054912 (2014) doi:10.1103/PhysRevC.90.054912 [arXiv:1405.7252 [hep-ph]].
- [54] B. B. Abelev *et al.* [ALICE], “Multiplicity Dependence of Pion, Kaon, Proton and Lambda Production in p-Pb Collisions at $\sqrt{s_{NN}} = 5.02$ TeV,” *Phys. Lett. B* **728**, 25-38 (2014) doi:10.1016/j.physletb.2013.11.020 [arXiv:1307.6796 [nucl-ex]].
- [55] A. Adare *et al.* [PHENIX], “Identified charged hadron production in $p + p$ collisions at $\sqrt{s} = 200$ and 62.4 GeV,” *Phys. Rev. C* **83**, 064903 (2011) doi:10.1103/PhysRevC.83.064903 [arXiv:1102.0753 [nucl-ex]].
- [56] J. Adams *et al.* [STAR], “ ϕ meson production in Au + Au and p+p collisions at $s(NN)^{(1/2)} = 200$ -GeV,” *Phys. Lett. B* **612**, 181-189 (2005) doi:10.1016/j.physletb.2004.12.082 [arXiv:nucl-ex/0406003 [nucl-ex]].
- [57] B. I. Abelev *et al.* [STAR], “Strange particle production in p+p collisions at $s^{*}(1/2) = 200$ -GeV,” *Phys. Rev. C* **75**, 064901 (2007) doi:10.1103/PhysRevC.75.064901 [arXiv:nucl-ex/0607033 [nucl-ex]].
- [58] A. Baran, W. Broniowski and W. Florkowski, “Description of the particle ratios and transverse momentum spectra for various centralities at RHIC in a single freeze-out model,” *Acta Phys. Polon. B* **35**, 779-798 (2004) [arXiv:nucl-th/0305075 [nucl-th]].
- [59] M. Shao, L. Yi, Z. Tang, H. Chen, C. Li and Z. Xu, “Examine the species and beam-energy dependence of particle spectra using Tsallis Statistics,” *J. Phys. G* **37**, 085104 (2010) doi:10.1088/0954-3899/37/8/085104 [arXiv:0912.0993 [nucl-ex]].
- [60] Waqas, M.; Chen, H.M.; Peng, G.X.; Haj Ismail, A.; Ajaz, M.; Wazir, Z.; Shehzadi, R.; Jamal, S.; AbdelKader, A. ”Study of Kinetic Freeze-Out Parameters as a Function of Rapidity in pp Collisions at CERN SPS Energies.” *Entropy* **23**, 1363 (2021). doi: 10.3390/e23101363
- [61] L. J. Gutay, A. S. Hirsch, C. Pajares, R. P. Scharenberg and B. K. Srivastava, “De-Confinement in small systems: Clustering of color sources in high multiplicity $\bar{p}p$ collisions at $\sqrt{s}= 1.8$ TeV,” *Int. J. Mod. Phys. E* **24**, no.12, 1550101 (2015) doi:10.1142/S0218301315501013 [arXiv:1504.08270 [nucl-ex]].
- [62] P. Sahoo, S. De, S. K. Tiwari and R. Sahoo, “Energy and Centrality Dependent Study of Deconfinement Phase Transition in a Color String Percolation Approach at RHIC Energies,” *Eur. Phys. J. A* **54**, no.8, 136 (2018) doi:10.1140/epja/i2018-12571-9 [arXiv:1803.08280 [hep-ph]].
- [63] R. P. Scharenberg, B. K. Srivastava and C. Pajares, “Exploring the initial stage of high multiplicity proton-proton collisions by determining the initial temperature of the quark-gluon plasma,” *Phys. Rev. D* **100**, no.11, 114040 (2019) doi:10.1103/PhysRevD.100.114040 [arXiv:1803.02301 [hep-ph]].
- [64] M. Ajaz, et al., ”Centrality dependence of P_T distribu-

tions and nuclear modification factor of charged particles in Pb-Pb interactions at $\sqrt{S_{NN}} = 2.76$ TeV.” Results Phys. **30**, 104790 (2021). doi:10.1016/j.rinp.2021.104790
 [65] M. Waqas and G. X. Peng, “Study of Proton,

Deuteron, and Triton at 54.4 GeV,” Adv. High Energy Phys. **2021**, 6674470 (2021) doi:10.1155/2021/6674470 [arXiv:2103.07852 [hep-ph]].

Table 1. Values of free parameters (T and q), normalization constant (σ_0), χ^2 , and ndof corresponding to the curves in Figure 1 for pp collisions at 200 GeV, where the spectrum form and particle mass are given together. In the last column, “-” for ndof denotes the case which has the number of data points being less than or equal to 0 and the curve is only to guide the eyes. After rounding, the value of χ^2 is taken to be an integer. If the integer is 0, we keep one decimal; If the one decimal is 0.0, we keep two decimals, and so on.

Collisions	Centrality	Particle	T_0 (GeV)	β_T (c)	$V(fm^3)$	n	N_0	χ^2/dof
200 GeV	Fig. 1 0-10%	π^+	0.057 ± 0.006	0.309 ± 0.012	2200 ± 150	10 ± 1	55 ± 3	0.5/8
	Cu-Cu 10-30%	-	0.052 ± 0.005	0.309 ± 0.009	2100 ± 130	10 ± 1.2	33 ± 2	0.6/8
	30-50%	-	0.049 ± 0.005	0.309 ± 0.010	2000 ± 130	10 ± 1	14 ± 1	1.5/8
	50-70%	-	0.045 ± 0.004	0.309 ± 0.010	1874 ± 114	10 ± 1.2	5.8 ± 0.8	0.5/8
	0-10%	π^-	0.057 ± 0.006	0.309 ± 0.012	2200 ± 150	10 ± 1	55 ± 3	0.5/8
	10-30%	-	0.052 ± 0.005	0.309 ± 0.009	2100 ± 130	10 ± 1.2	33 ± 2	0.6/8
	30-50%	-	0.049 ± 0.005	0.309 ± 0.010	2000 ± 130	10 ± 1	14 ± 1	1.5/8
	50-70%	-	0.045 ± 0.004	0.309 ± 0.010	1874 ± 114	10 ± 1.2	5.8 ± 0.8	0.5/8
	0-10%	K^+	0.076 ± 0.004	0.289 ± 0.009	2050 ± 110	11 ± 1.4	0.036 ± 0.005	2/7
	10-30%	-	0.072 ± 0.004	0.289 ± 0.008	1938 ± 106	11 ± 1.3	0.009 ± 0.0005	4/7
	30-50%	-	0.064 ± 0.006	0.289 ± 0.009	1841 ± 116	11 ± 1.2	$3.8 \times 10^{-3} \pm 5 \times 10^{-4}$	3/7
	50-70%	-	0.060 ± 0.004	0.289 ± 0.010	1741 ± 111	11 ± 1.2	$3.5 \times 10^{-3} \pm 5 \times 10^{-4}$	8/7
	0-10%	K^-	0.076 ± 0.004	0.289 ± 0.009	2050 ± 110	11 ± 1.4	0.036 ± 0.005	2/7
	10-30%	-	0.072 ± 0.004	0.289 ± 0.008	1938 ± 106	11 ± 1.3	0.009 ± 0.0005	4/7
	30-50%	-	0.064 ± 0.006	0.289 ± 0.009	1841 ± 116	11 ± 1.2	$3.8 \times 10^{-3} \pm 5 \times 10^{-4}$	3/7
	50-70%	-	0.060 ± 0.004	0.289 ± 0.010	1741 ± 111	11 ± 1.2	$3.5 \times 10^{-3} \pm 5 \times 10^{-4}$	8/7
	0-10%	p	0.058 ± 0.006	0.267 ± 0.012	1857 ± 123	15 ± 1.7	$8 \times 10^{-5} \pm 6 \times 10^{-6}$	17/8
	10-30%	-	0.053 ± 0.005	0.267 ± 0.010	1730 ± 124	15 ± 2	$5 \times 10^{-5} \pm 4 \times 10^{-6}$	22/8
	30-50%	-	0.050 ± 0.004	0.267 ± 0.010	1600 ± 126	15 ± 2	$2 \times 10^{-5} \pm 4 \times 10^{-6}$	17/8
	50-70%	-	0.046 ± 0.005	0.267 ± 0.010	1500 ± 130	15 ± 2.1	$7 \times 10^{-6} \pm 4 \times 10^{-7}$	43/8
	0-10%	\bar{p}	0.058 ± 0.006	0.267 ± 0.012	1857 ± 123	15 ± 1.7	$8 \times 10^{-5} \pm 6 \times 10^{-6}$	17/8
	10-30%	-	0.053 ± 0.005	0.267 ± 0.010	1730 ± 124	15 ± 2	$5 \times 10^{-5} \pm 4 \times 10^{-6}$	22/8
	30-50%	-	0.050 ± 0.004	0.267 ± 0.010	1600 ± 126	15 ± 2	$2 \times 10^{-5} \pm 4 \times 10^{-6}$	17/8
	50-70%	-	0.046 ± 0.005	0.267 ± 0.010	1500 ± 130	15 ± 2.1	$7 \times 10^{-6} \pm 4 \times 10^{-7}$	43/8
	0-10%	Λ	0.076 ± 0.005	0.254 ± 0.010	1713 ± 108	15.4 ± 1.5	2.4 ± 0.3	22/14
	10-20%	-	0.072 ± 0.004	0.254 ± 0.010	1610 ± 104	15.4 ± 1.8	0.165 ± 0.03	29/14
	20-30%	-	0.068 ± 0.004	0.254 ± 0.011	1500 ± 111	15.4 ± 2.1	0.012 ± 0.004	20/14
	30-40%	-	0.064 ± 0.004	0.254 ± 0.011	1410 ± 120	15.4 ± 2.2	$8 \times 10^{-4} \pm 5 \times 10^{-5}$	31/14
	40-60%	-	0.060 ± 0.006	0.254 ± 0.010	1300 ± 120	15.4 ± 2.2	$4.3 \times 10^{-5} \pm 4 \times 10^{-6}$	14/14
	0-10%	Ξ	0.076 ± 0.004	0.244 ± 0.009	1500 ± 115	15.5 ± 1.5	0.24 ± 0.04	25/6
	10-20%	-	0.072 ± 0.004	0.244 ± 0.010	1420 ± 104	15.5 ± 2.2	0.016 ± 0.005	10/6
	20-30%	-	0.069 ± 0.004	0.244 ± 0.012	1290 ± 126	15.5 ± 2.2	0.001 ± 0.0004	33/6
	30-40%	-	0.065 ± 0.005	0.244 ± 0.011	1200 ± 100	15.5 ± 2.2	$8 \times 10^{-5} \pm 5 \times 10^{-6}$	17/6
	40-60%	-	0.061 ± 0.004	0.244 ± 0.011	1120 ± 100	15.5 ± 2.2	$4 \times 10^{-6} \pm 6 \times 10^{-7}$	15/6
62.4 GeV	Fig. 2 0-5%	π^+	0.060 ± 0.005	0.325 ± 0.012	2357 ± 170	10.4 ± 1.5	270 ± 32	0.2/5
	Au-Au 5-10%	-	0.056 ± 0.006	0.325 ± 0.010	2268 ± 140	10.4 ± 1.5	210 ± 18	0.8/5
	10-20%	-	0.052 ± 0.004	0.325 ± 0.010	2150 ± 130	10.4 ± 1	170 ± 10	0.5/5
	20-30%	-	0.048 ± 0.005	0.325 ± 0.010	2035 ± 120	10.4 ± 2	146 ± 8	0.5/5
	30-40%	-	0.045 ± 0.006	0.325 ± 0.011	1955 ± 110	10.4 ± 1.5	106 ± 10	1.3/5
	40-50%	-	0.042 ± 0.005	0.325 ± 0.011	1775 ± 132	10.4 ± 1.2	62 ± 8	1.5/5
	50-60%	-	0.040 ± 0.004	0.325 ± 0.009	1702 ± 108	10.4 ± 1.8	38 ± 4	2.5/5
	60-70%	-	0.037 ± 0.004	0.325 ± 0.011	1620 ± 110	10.4 ± 1.6	21.7 ± 3.5	5.5/5
	70-80%	-	0.034 ± 0.004	0.325 ± 0.011	1530 ± 88	10.8 ± 1.6	11.6 ± 2	2.5/5
	0-5%	K^+	0.076 ± 0.006	0.312 ± 0.010	2100 ± 120	11 ± 1.5	26.4 ± 3.8	4/5
	5-10%	-	0.073 ± 0.006	0.312 ± 0.010	2000 ± 100	11 ± 1.3	22.4 ± 1.3	3/5
	10-20%	-	0.070 ± 0.005	0.312 ± 0.011	1900 ± 100	11 ± 1.4	17.7 ± 2	5/5
	20-30%	-	0.067 ± 0.005	0.312 ± 0.011	1813 ± 104	11 ± 1.2	13 ± 2	4/5
	30-40%	-	0.064 ± 0.005	0.312 ± 0.010	1730 ± 108	11 ± 1.4	9.2 ± 1.4	4/5

Table 1. Continue.

Collisions	Centrality	Particle	T_0 (GeV)	β_T (c)	$V(fm^3)$	n	N_0	χ^2/dof
Fig. 3 d-Au 200 GeV	0–5%	p	0.060 ± 0.005	0.280 ± 0.010	1930 ± 108	8.4 ± 1	7 ± 0.8	9/9
	5–10%	–	0.056 ± 0.005	0.280 ± 0.011	1843 ± 110	9 ± 0.6	6.1 ± 0.6	2/9
	10–20%	–	0.053 ± 0.005	0.280 ± 0.009	1739 ± 120	9 ± 0.4	5 ± 0.5	1/9
	20–30%	–	0.049 ± 0.004	0.280 ± 0.010	1627 ± 109	9 ± 1	3.7 ± 0.4	3/9
	30–40%	–	0.045 ± 0.006	0.280 ± 0.012	1500 ± 100	11 ± 1	2.8 ± 0.5	2/9
	40–50%	–	0.042 ± 0.005	0.280 ± 0.012	1385 ± 100	11.5 ± 1.5	1.95 ± 0.3	2/9
	50–60%	–	0.040 ± 0.005	0.280 ± 0.011	1300 ± 93	13 ± 1.6	1.3 ± 0.04	1/9
	60–70%	–	0.038 ± 0.004	0.280 ± 0.010	1212 ± 80	15 ± 1.4	0.745 ± 0.04	3/9
	70–80%	–	0.035 ± 0.005	0.280 ± 0.010	1100 ± 60	16 ± 1.5	0.37 ± 0.03	4/9
	0–5%	Λ	0.076 ± 0.006	0.260 ± 0.012	1800 ± 126	15 ± 1.5	7.6 ± 0.5	5/7
	5–10%	–	0.073 ± 0.006	0.260 ± 0.009	1700 ± 100	15 ± 1.6	0.61 ± 0.06	11/7
	10–20%	–	0.070 ± 0.006	0.260 ± 0.011	1610 ± 100	15 ± 1.5	0.058 ± 0.005	8/7
	20–30%	–	0.067 ± 0.005	0.260 ± 0.013	1523 ± 96	15 ± 1.7	0.0033 ± 0.0004	8/7
	30–40%	–	0.064 ± 0.005	0.260 ± 0.010	1450 ± 70	15 ± 1.4	$2.5 \times 10^{-4} \pm 4 \times 10^{-5}$	3/7
	40–60%	–	0.060 ± 0.004	0.260 ± 0.011	1329 ± 80	15 ± 1.6	$9.4 \times 10^{-6} \pm 5 \times 10^{-7}$	16/7
	60–80%	–	0.055 ± 0.004	0.260 ± 0.010	1200 ± 85	15 ± 1.6	$2.9 \times 10^{-7} \pm 4 \times 10^{-8}$	3/7
	0–5%	Ξ^-	0.076 ± 0.006	0.249 ± 0.012	1680 ± 100	13 ± 1.2	0.33 ± 0.04	2/5
	5–10%	–	0.073 ± 0.006	0.249 ± 0.009	1600 ± 100	14 ± 1.2	0.033 ± 0.004	4/5
	10–20%	–	0.070 ± 0.006	0.249 ± 0.011	1500 ± 80	14 ± 1.3	0.0024 ± 0.0005	4/5
	20–30%	–	0.067 ± 0.005	0.249 ± 0.013	1400 ± 70	14 ± 1.5	$1.6 \times 10^{-4} \pm 5 \times 10^{-5}$	1.5/5
	30–40%	–	0.064 ± 0.005	0.249 ± 0.010	1320 ± 70	15 ± 1.5	$4.4 \times 10^{-6} \pm 5 \times 10^{-7}$	3/5
	40–60%	–	0.060 ± 0.004	0.249 ± 0.011	1200 ± 80	15 ± 1.5	$1.4 \times 10^{-7} \pm 5 \times 10^{-8}$	1.5/5
	0–20%	π^+	0.058 ± 0.004	0.315 ± 0.009	2250 ± 100	9.8 ± 1.3	0.075 ± 0.005	2/19
	20–40%	–	0.055 ± 0.004	0.315 ± 0.009	2170 ± 104	9.8 ± 1.3	0.006 ± 0.0004	2/19
	40–60%	–	0.048 ± 0.005	0.315 ± 0.011	1954 ± 110	9.8 ± 1.2	$5 \times 10^{-5} \pm 5 \times 10^{-6}$	0.6/19
	60–80%	–	0.044 ± 0.004	0.315 ± 0.009	1843 ± 123	9.8 ± 1.4	$1.8 \times 10^{-6} \pm 4 \times 10^{-7}$	3/19
	0–20%	π^-	0.058 ± 0.004	0.315 ± 0.009	2250 ± 100	9.8 ± 1.3	0.075 ± 0.005	2/19
	20–40%	–	0.055 ± 0.004	0.315 ± 0.009	2170 ± 104	9.8 ± 1.3	0.006 ± 0.0004	2/19
	40–60%	–	0.048 ± 0.005	0.315 ± 0.011	1954 ± 110	9.8 ± 1.2	$5 \times 10^{-5} \pm 5 \times 10^{-6}$	0.6/19
	60–80%	–	0.044 ± 0.004	0.315 ± 0.009	1843 ± 123	9.8 ± 1.4	$1.8 \times 10^{-6} \pm 4 \times 10^{-7}$	3/19
	0–20%	K^+	0.078 ± 0.005	0.296 ± 0.010	2119 ± 110	9.4 ± 1.2	0.0055 ± 0.0005	1.4/14
	20–40%	–	0.074 ± 0.006	0.296 ± 0.011	2041 ± 121	9.4 ± 1.4	$4.1 \times 10^{-4} \pm 5 \times 10^{-5}$	1/14
	40–60%	–	0.067 ± 0.006	0.296 ± 0.013	1817 ± 116	9.4 ± 1.4	$3.6 \times 10^{-6} \pm 5 \times 10^{-7}$	1/14
	60–80%	–	0.062 ± 0.005	0.296 ± 0.011	1703 ± 120	9.8 ± 1.1	$1.4 \times 10^{-7} \pm 6 \times 10^{-8}$	3/14
	0–20%	K^-	0.078 ± 0.005	0.296 ± 0.010	2119 ± 110	9.4 ± 1.2	0.0055 ± 0.0005	1.4/14
	20–40%	–	0.074 ± 0.006	0.296 ± 0.011	2041 ± 121	9.4 ± 1.4	$4.1 \times 10^{-4} \pm 5 \times 10^{-5}$	1/14
	40–60%	–	0.067 ± 0.006	0.296 ± 0.013	1817 ± 116	9.4 ± 1.4	$3.6 \times 10^{-6} \pm 5 \times 10^{-7}$	1/14
	60–80%	–	0.062 ± 0.005	0.296 ± 0.011	1703 ± 120	9.8 ± 1.1	$1.4 \times 10^{-7} \pm 6 \times 10^{-8}$	3/14
	0–20%	p	0.061 ± 0.006	0.283 ± 0.008	1920 ± 109	11 ± 1.5	$7.3 \times 10^{-4} \pm 6 \times 10^{-5}$	4.5/19
	20–40%	–	0.057 ± 0.004	0.283 ± 0.010	1834 ± 101	11 ± 1.5	$5.5 \times 10^{-5} \pm 5 \times 10^{-6}$	2/19
	40–60%	–	0.048 ± 0.005	0.283 ± 0.011	1600 ± 106	11 ± 1.2	$5.1 \times 10^{-7} \pm 4 \times 10^{-8}$	1/19
	60–80%	–	0.045 ± 0.004	0.283 ± 0.010	1500 ± 102	12 ± 1.4	$2.4 \times 10^{-8} \pm 5 \times 10^{-9}$	2/19
	0–20%	\bar{p}	0.061 ± 0.006	0.283 ± 0.008	1920 ± 109	11 ± 1.5	$7.3 \times 10^{-4} \pm 6 \times 10^{-5}$	4.5/19
	20–40%	–	0.057 ± 0.004	0.283 ± 0.010	1834 ± 101	11 ± 1.5	$5.5 \times 10^{-5} \pm 5 \times 10^{-6}$	2/19
	40–60%	–	0.048 ± 0.005	0.283 ± 0.011	1600 ± 106	11 ± 1.2	$5.1 \times 10^{-7} \pm 4 \times 10^{-8}$	1/19
	60–80%	–	0.045 ± 0.004	0.283 ± 0.010	1500 ± 102	12 ± 1.4	$2.4 \times 10^{-8} \pm 5 \times 10^{-9}$	2/19

Table 1. Continue.

Collisions	Centrality	Particle	T_0 (GeV)	β_T (c)	$V(fm^3)$	n	N_0	χ^2/dof
Fig. 4 Pb-Pb 2.76 TeV	0–5%	π^+	0.108 ± 0.005	0.443 ± 0.011	3500 ± 140	9.8 ± 1	$2.3 \times 10^5 \pm 5 \times 10^4$	34/36
	5–10%	–	0.104 ± 0.004	0.443 ± 0.010	3360 ± 143	9.8 ± 1	$1.1 \times 10^5 \pm 4 \times 10^4$	40/36
	10–20%		0.100 ± 0.005	0.443 ± 0.010	3237 ± 136	9.8 ± 1.2	$4 \times 10^4 \pm 6 \times 10^3$	21/36
	20–30%	–	0.096 ± 0.006	0.443 ± 0.012	3100 ± 124	9.8 ± 1.3	$1.4 \times 10^4 \pm 4 \times 10^3$	29/36
	30–40%	–	0.092 ± 0.006	0.443 ± 0.010	2974 ± 109	9.8 ± 1	$5 \times 10^3 \pm 5 \times 10^2$	40/36
	40–50%	–	0.089 ± 0.004	0.443 ± 0.012	2854 ± 108	9.8 ± 1	$1.6 \times 10^3 \pm 3 \times 10^2$	35/36
	50–60%	–	0.086 ± 0.005	0.443 ± 0.010	2719 ± 120	9.8 ± 1.1	450 ± 21	34/36
	60–70%	–	0.082 ± 0.006	0.443 ± 0.012	2600 ± 132	10.3 ± 1.3	150 ± 10	55/36
	70–80%	–	0.078 ± 0.004	0.443 ± 0.012	2500 ± 100	10.3 ± 1.2	34 ± 4	71/36
	80–90%	–	0.074 ± 0.005	0.443 ± 0.010	2300 ± 161	10.3 ± 1.4	7.5 ± 0.4	73/36
	0–5%	π^-	0.108 ± 0.005	0.443 ± 0.011	3500 ± 140	9.8 ± 1	$2.3 \times 10^5 \pm 5 \times 10^4$	34/36
	5–10%	–	0.104 ± 0.004	0.443 ± 0.010	3360 ± 143	9.8 ± 1	$1.1 \times 10^5 \pm 4 \times 10^4$	40/36
	10–20%		0.100 ± 0.005	0.443 ± 0.010	3237 ± 136	9.8 ± 1.2	$4 \times 10^4 \pm 6 \times 10^3$	21/36
	20–30%	–	0.096 ± 0.006	0.443 ± 0.012	3100 ± 124	9.8 ± 1.3	$1.4 \times 10^4 \pm 4 \times 10^3$	29/36
	30–40%	–	0.092 ± 0.006	0.443 ± 0.010	2974 ± 109	9.8 ± 1	$5 \times 10^3 \pm 5 \times 10^2$	40/36
	40–50%	–	0.089 ± 0.004	0.443 ± 0.012	2854 ± 108	9.8 ± 1	$1.6 \times 10^3 \pm 3 \times 10^2$	35/36
	50–60%	–	0.086 ± 0.005	0.443 ± 0.010	2719 ± 120	9.8 ± 1.1	450 ± 21	34/36
	60–70%	–	0.082 ± 0.006	0.443 ± 0.012	2600 ± 132	10.3 ± 1.3	150 ± 10	55/36
	70–80%	–	0.078 ± 0.004	0.443 ± 0.012	2500 ± 100	10.3 ± 1.2	34 ± 4	71/36
	80–90%	–	0.074 ± 0.005	0.443 ± 0.010	2300 ± 161	10.3 ± 1.4	7.5 ± 0.4	73/36
	0–5%	K^+	0.129 ± 0.004	0.421 ± 0.009	3319 ± 138	9.3 ± 1.2	$1.9 \times 10^4 \pm 4 \times 10^3$	40/31
	5–10%	–	0.126 ± 0.004	0.421 ± 0.009	3319 ± 138	9.3 ± 1.2	$8.6 \times 10^3 \pm 5 \times 10^2$	24/31
	10–20%		0.122 ± 0.005	0.421 ± 0.011	3200 ± 180	9.3 ± 1.3	$3.3 \times 10^3 \pm 5 \times 10^2$	25/31
	20–30%	–	0.119 ± 0.006	0.421 ± 0.010	3000 ± 181	9.3 ± 1.3	$1.2 \times 10^3 \pm 4 \times 10^2$	17/31
	30–40%	–	0.115 ± 0.005	0.421 ± 0.012	2875 ± 130	9.3 ± 1.3	400 ± 24	10/31
	40–50%	–	0.110 ± 0.006	0.421 ± 0.011	2732 ± 131	9.3 ± 1.4	130 ± 10	16/31
	50–60%	–	0.107 ± 0.005	0.421 ± 0.010	2600 ± 126	9.3 ± 1.4	36 ± 5	20/31
	60–70%	–	0.102 ± 0.004	0.421 ± 0.012	2450 ± 142	9.5 ± 1.3	10 ± 0.4	12/31
	70–80%	–	0.098 ± 0.005	0.421 ± 0.010	2350 ± 126	9.8 ± 1.3	2.5 ± 0.3	65/31
	80–90%	–	0.094 ± 0.005	0.421 ± 0.011	2220 ± 141	10 ± 1.4	0.5 ± 0.03	35/31
	0–5%	K^-	0.129 ± 0.004	0.421 ± 0.009	3319 ± 138	9.3 ± 1.2	$1.9 \times 10^4 \pm 4 \times 10^3$	40/31
	5–10%	–	0.126 ± 0.004	0.421 ± 0.009	3319 ± 138	9.3 ± 1.2	$8.6 \times 10^3 \pm 5 \times 10^2$	24/31
	10–20%		0.122 ± 0.005	0.421 ± 0.011	3200 ± 180	9.3 ± 1.3	$3.3 \times 10^3 \pm 5 \times 10^2$	25/31
	20–30%	–	0.119 ± 0.006	0.421 ± 0.010	3000 ± 181	9.3 ± 1.3	$1.2 \times 10^3 \pm 4 \times 10^2$	17/31
	30–40%	–	0.115 ± 0.005	0.421 ± 0.012	2875 ± 130	9.3 ± 1.3	400 ± 24	10/31
	40–50%	–	0.110 ± 0.006	0.421 ± 0.011	2732 ± 131	9.3 ± 1.4	130 ± 10	16/31
	50–60%	–	0.107 ± 0.005	0.421 ± 0.010	2600 ± 126	9.3 ± 1.4	36 ± 5	20/31
	60–70%	–	0.102 ± 0.004	0.421 ± 0.012	2450 ± 142	9.5 ± 1.3	10 ± 0.4	12/31
	70–80%	–	0.098 ± 0.005	0.421 ± 0.010	2350 ± 126	9.8 ± 1.3	2.5 ± 0.3	65/31
	80–90%	–	0.094 ± 0.005	0.421 ± 0.011	2220 ± 141	10 ± 1.4	0.5 ± 0.03	35/31
	0–5%	p	0.108 ± 0.005	0.403 ± 0.010	3100 ± 140	9.8 ± 1	$2.3 \times 10^5 \pm 5 \times 10^4$	34/32
	5–10%	–	0.104 ± 0.006	0.403 ± 0.011	2900 ± 142	9 ± 1.2	1000 ± 100	151/32
	10–20%		0.101 ± 0.004	0.403 ± 0.010	2768 ± 120	9 ± 1.2	400 ± 20	151/32
	20–30%	–	0.097 ± 0.005	0.403 ± 0.010	2550 ± 136	9 ± 1.2	150 ± 10	148/32
	30–40%	–	0.094 ± 0.005	0.403 ± 0.010	2400 ± 130	9 ± 1.1	47 ± 4	143/32

Table 1. Continue.

Collisions	Centrality	Particle	T_0 (GeV)	β_T (c)	$V(fm^3)$	n	N_0	χ^2/dof
Fig. 5 p-Pb 5.02 TeV	40–50%	–	0.090 ± 0.005	0.403 ± 0.011	2300 ± 140	9.8 ± 1.3	17 ± 2	43/32
	50–60%	–	0.086 ± 0.004	0.403 ± 0.012	2200 ± 100	10.3 ± 1.1	5.5 ± 0.5	17/32
	60–70%	–	0.083 ± 0.005	0.403 ± 0.012	2050 ± 110	10.3 ± 1.1	1.6 ± 0.3	35/32
	70–80%	–	0.080 ± 0.006	0.403 ± 0.012	1910 ± 120	10.7 ± 1.4	0.38 ± 0.02	54/32
	80–90%	–	0.077 ± 0.004	0.403 ± 0.010	1800 ± 100	11.7 ± 1.2	0.08 ± 0.003	61/32
	0–5%	\bar{p}	0.108 ± 0.005	0.403 ± 0.010	3100 ± 140	9.8 ± 1	$2.3 \times 10^5 \pm 5 \times 10^4$	34/32
	5–10%	–	0.104 ± 0.006	0.403 ± 0.011	2900 ± 142	9 ± 1.2	1000 ± 100	151/32
	10–20%	–	0.101 ± 0.004	0.403 ± 0.010	2768 ± 120	9 ± 1.2	400 ± 20	151/32
	20–30%	–	0.097 ± 0.005	0.403 ± 0.010	2550 ± 136	9 ± 1.2	150 ± 10	148/32
	30–40%	–	0.094 ± 0.005	0.403 ± 0.010	2400 ± 130	9 ± 1.1	47 ± 4	143/32
	40–50%	–	0.090 ± 0.005	0.403 ± 0.011	2300 ± 140	9.8 ± 1.3	17 ± 2	43/32
	50–60%	–	0.086 ± 0.004	0.403 ± 0.012	2200 ± 100	10.3 ± 1.1	5.5 ± 0.5	17/32
	60–70%	–	0.083 ± 0.005	0.403 ± 0.012	2050 ± 110	10.3 ± 1.1	1.6 ± 0.3	35/32
	70–80%	–	0.080 ± 0.006	0.403 ± 0.012	1910 ± 120	10.7 ± 1.4	0.38 ± 0.02	54/32
	80–90%	–	0.077 ± 0.004	0.403 ± 0.010	1800 ± 100	11.7 ± 1.2	0.08 ± 0.003	61/32
	0–10%	Λ	0.128 ± 0.005	0.381 ± 0.010	2900 ± 150	7 ± 0.7	17 ± 2	130/14
	10–20%	–	0.126 ± 0.006	0.381 ± 0.010	2750 ± 100	7 ± 1	13 ± 0.4	74/14
	20–40%	–	0.120 ± 0.005	0.381 ± 0.011	2623 ± 110	7.3 ± 1.1	7.9 ± 0.2	105/14
	40–60%	–	0.111 ± 0.006	0.381 ± 0.012	2500 ± 130	9.4 ± 1.2	3.5 ± 0.2	22/14
	60–80%	–	0.105 ± 0.005	0.381 ± 0.012	2400 ± 152	10.5 ± 1.3	1 ± 0.02	20/14
	0–10%	Ξ	0.128 ± 0.006	0.287 ± 0.012	2600 ± 180	7 ± 0.6	5.5 ± 0.3	39/7
	10–20%	–	0.125 ± 0.004	0.287 ± 0.012	2477 ± 150	7 ± 0.5	4.2 ± 0.4	25/7
	20–40%	–	0.120 ± 0.004	0.287 ± 0.010	2356 ± 144	7.6 ± 0.4	2.7 ± 0.2	13/7
	40–60%	–	0.112 ± 0.005	0.287 ± 0.011	2207 ± 108	8 ± 0.4	1 ± 0.2	32/7
	60–80%	–	0.105 ± 0.004	0.287 ± 0.010	2100 ± 120	10 ± 0.8	0.3 ± 0.03	57/7
	0–5%	$\pi^+ + \pi^-$	0.100 ± 0.006	0.430 ± 0.010	3300 ± 150	9 ± 1	1700 ± 113	67/36
	5–10%	–	0.096 ± 0.005	0.430 ± 0.011	3200 ± 136	9 ± 1	700 ± 100	51/36
	10–20%	–	0.092 ± 0.004	0.430 ± 0.012	3100 ± 124	9 ± 1.2	300 ± 13	44/36
	20–40%	–	0.088 ± 0.005	0.430 ± 0.011	2942 ± 156	9 ± 1.1	130 ± 16	49/36
	40–60%	–	0.083 ± 0.006	0.430 ± 0.009	2800 ± 140	9 ± 1.2	37 ± 7	42/36
	60–80%	–	0.079 ± 0.005	0.430 ± 0.011	2647 ± 137	9.7 ± 1.3	17 ± 3	82/36
	80–100%	–	0.075 ± 0.005	0.430 ± 0.011	2500 ± 141	10 ± 1.2	3.6 ± 0.5	67/36
	0–5%	$K^+ + K^-$	0.120 ± 0.005	0.400 ± 0.011	3100 ± 145	8 ± 0.7	128 ± 13	5/26
	5–10%	–	0.116 ± 0.006	0.400 ± 0.012	2974 ± 130	8 ± 0.5	52 ± 4	8/26
	10–20%	–	0.112 ± 0.005	0.400 ± 0.012	2851 ± 140	8.2 ± 0.6	23 ± 3	45/26
	20–40%	–	0.108 ± 0.005	0.400 ± 0.011	2714 ± 124	8.2 ± 0.5	10 ± 0.4	10/26
	40–60%	–	0.104 ± 0.005	0.400 ± 0.010	2600 ± 108	8.6 ± 0.6	5.2 ± 0.4	21/26
	60–80%	–	0.100 ± 0.005	0.400 ± 0.010	2500 ± 100	9 ± 0.7	1.2 ± 0.04	45/26
	80–100%	–	0.096 ± 0.004	0.400 ± 0.011	2400 ± 100	10.6 ± 1	0.3 ± 0.03	90/26
	0–5%	$p + \bar{p}$	0.100 ± 0.004	0.380 ± 0.012	2928 ± 140	8.4 ± 0.8	20 ± 2	9/34
	5–10%	–	0.096 ± 0.005	0.380 ± 0.010	2800 ± 120	8.4 ± 0.6	8.7 ± 0.6	14/34
	10–20%	–	0.092 ± 0.005	0.380 ± 0.010	2700 ± 130	8.4 ± 0.6	3.5 ± 0.2	50/34
	20–40%	–	0.088 ± 0.006	0.380 ± 0.010	2570 ± 110	8.9 ± 0.8	1.8 ± 0.03	86/34
	40–60%	–	0.084 ± 0.005	0.380 ± 0.011	2450 ± 109	9.5 ± 0.5	0.6 ± 0.02	6/34
	60–80%	–	0.080 ± 0.005	0.380 ± 0.011	2323 ± 108	10.5 ± 0.6	0.24 ± 0.02	28/34
	80–100%	–	0.078 ± 0.005	0.380 ± 0.010	2200 ± 100	12 ± 1	0.059 ± 0.003	91/34
	0–5%	$\Lambda + \bar{\Lambda}$	0.120 ± 0.006	0.330 ± 0.009	2500 ± 180	8.8 ± 0.4	15 ± 2	159/13
	5–10%	–	0.115 ± 0.006	0.330 ± 0.011	2350 ± 135	8.8 ± 0.3	7 ± 0.4	96/13
	10–20%	–	0.114 ± 0.004	0.330 ± 0.012	2220 ± 146	8.8 ± 0.4	3 ± 0.2	110/13
	20–40%	–	0.110 ± 0.005	0.330 ± 0.012	2220 ± 142	9 ± 0.35	1.15 ± 0.05	32/13
	40–60%	–	0.105 ± 0.004	0.330 ± 0.010	2100 ± 136	9 ± 0.5	0.4 ± 0.02	73/13
	60–80%	–	0.101 ± 0.005	0.330 ± 0.012	2000 ± 150	9.9 ± 0.7	0.14 ± 0.02	136/13

Table 1. Continue.

Collisions	Centrality	Particle	T_0 (GeV)	β_T (c)	$V(fm^3)$	n	N_0	χ^2/dof
p-p 200 GeV	—	π^+	0.042 ± 0.006	0.256 ± 0.008	532 ± 30	8 ± 0.4	63 ± 3	9/22
	—	π^-	0.042 ± 0.006	0.256 ± 0.008	532 ± 30	8 ± 0.4	63 ± 3	9/22
	—	K^+	0.050 ± 0.004	0.230 ± 0.009	434 ± 30	8 ± 0.4	10 ± 0.3	8/11
	—	K^-	0.050 ± 0.004	0.230 ± 0.009	434 ± 30	8 ± 0.4	10 ± 0.3	8/11
	—	p	0.042 ± 0.005	0.214 ± 0.010	390 ± 31	9.8 ± 0.5	2 ± 0.2	9/28
	—	\bar{p}	0.042 ± 0.005	0.214 ± 0.010	390 ± 23	9.8 ± 0.5	2 ± 0.2	9/28
	—	ϕ	0.050 ± 0.006	0.200 ± 0.011	312 ± 21	8 ± 0.2	0.007 ± 0.0002	14/8
	—	Ξ^-	0.050 ± 0.005	0.187 ± 0.010	287 ± 21	8 ± 0.3	0.004 ± 0.0002	15/6